JOURNAL OF GEOPHYSICAL RESEARCH, VOL. 113, B02101, doi:10.1029/2007JB004736, 2008

Determination of magnetic properties of rocks by analysis of demagnetization curves: Hematite-ilmenite bearing rocks from SW Sweden

Erik Eneroth[1] and Leif Johansson[1]

Received 5 September 2006; revised 12 June 2007; accepted 13 August 2007; published 2 February 2008.

[1] Granulites from the high-grade Sveconorwegian (corresponding to Grenvillian) gneiss terrane of SW Sweden were investigated in order to relate magnetic properties to the granulite facies mineralogy and the amphibolite facies retrograde mineralogy. We used standard paleomagnetic techniques, susceptibility measurements, electron and optical microscopy, and a new way to analyze demagnetization curves based on vector difference sums. The new technique allowed quantitation of the relative contributions of partial natural remanent magnetization (NRM) components as well as numerical extraction of thermal and coercive force (alternating field, AF) unblocking data. Two major components were identified, one stable which is carried by hematite-ilmenite, and one less stable carried by multidomain (MD) magnetite. The age of the hematite-ilmenite component is circa 930 Ma, and it has steep negative inclination, coercivities in excess of 150 mT, and unblocking temperatures between 540°C and 640°C. Two corresponding poles are reported (1) paleolatitude/paleolongitude (plat/plong) (218°/−24.3°) with D_p/D_m (9.4°/9.9°) (paleopole) and (2) plat/plong (203°/−51°) with D_p/D_m (4.4°/5.6°) (VGP). The MD magnetite component is a recent or Cretaceous-Paleogene, steeply positive inclined NRM component associated with strong induced magnetization (plat/plong 2°/−74° and D_p/D_m 11°/14°) (VGP). The MD magnetite was unblocked at conditions of 6−40 mT and 60−400°C. Our new analysis method was successful in showing that retrograde amphibole formation strongly decreases the importance of the hematite-ilmenite component on behalf of the MD magnetite. It has a diminishing effect on a negative aeromagnetic anomaly in the area. The 930 Ma components constitute 80−0% of the vector difference sums depending on rock composition. However, as this fraction goes down to 60%, the induced magnetization seems to outweigh the hematite-ilmenite influence on aeromagnetic anomalies due to its opposite direction. These rocks still have a strong and stable hematite-ilmenite dominated NRM.

Citation: Eneroth, E., and L. Johansson (2008), Determination of magnetic properties of rocks by analysis of demagnetization curves: Hematite-ilmenite bearing rocks from SW Sweden, *J. Geophys. Res.*, *113*, B02101, doi:10.1029/2007JB004736.

1. Introduction

[2] Knowledge about remanent versus induced magnetization properties is critical for understanding anomalies in the earths magnetic field. The far most driven way to study magnetic anomalies is to make mathematical models showing the effects on the geomagnetic field due to magnetized rock formations in the crust [*Caratori Tontini*, 2005; *Pedersen*, 1985]. However, natural bedrock is often complex, and magnetic properties of rocks at depth in situ are largely unknown. Fortunately, the geological record contains evidence of metamorphic processes, which have occurred at depth and altered the magnetic properties. Then they have been uplifted to upper crustal levels (or even to the surface) where magnetic minerals are magnetically ordered. We can thus achieve at least a partial understanding of geomagnetic anomalies. In this article, we will describe magnetic properties of granulites from the eastern segment of the 980−930 Ma old Sveconorwegian domain in SW Sweden. Investigations were made with conventional demagnetization techniques combined with petrographical characterization and scanning electron microscopy. We also make an attempt to analyze the demagnetization curves, using new descriptive tools to assign numerical values to the demagnetization behaviors. The purpose is to define a more quantitative method to report rock magnetic data. Then we assess partial components to their correct ages using conventional paleopoles. Rock magnetic parameters, like NRM intensity, susceptibility (χ) and Koenigsberger ratio (Q) are also investigated in relation to variations in mineralogy. Exsolved hematite-ilmenite has been studied previously due

[1] GeoBiosphere Science Centre, Department of Geology, Lund University, Lund, Sweden.

0148-0227/08/2007JB004736$09.00

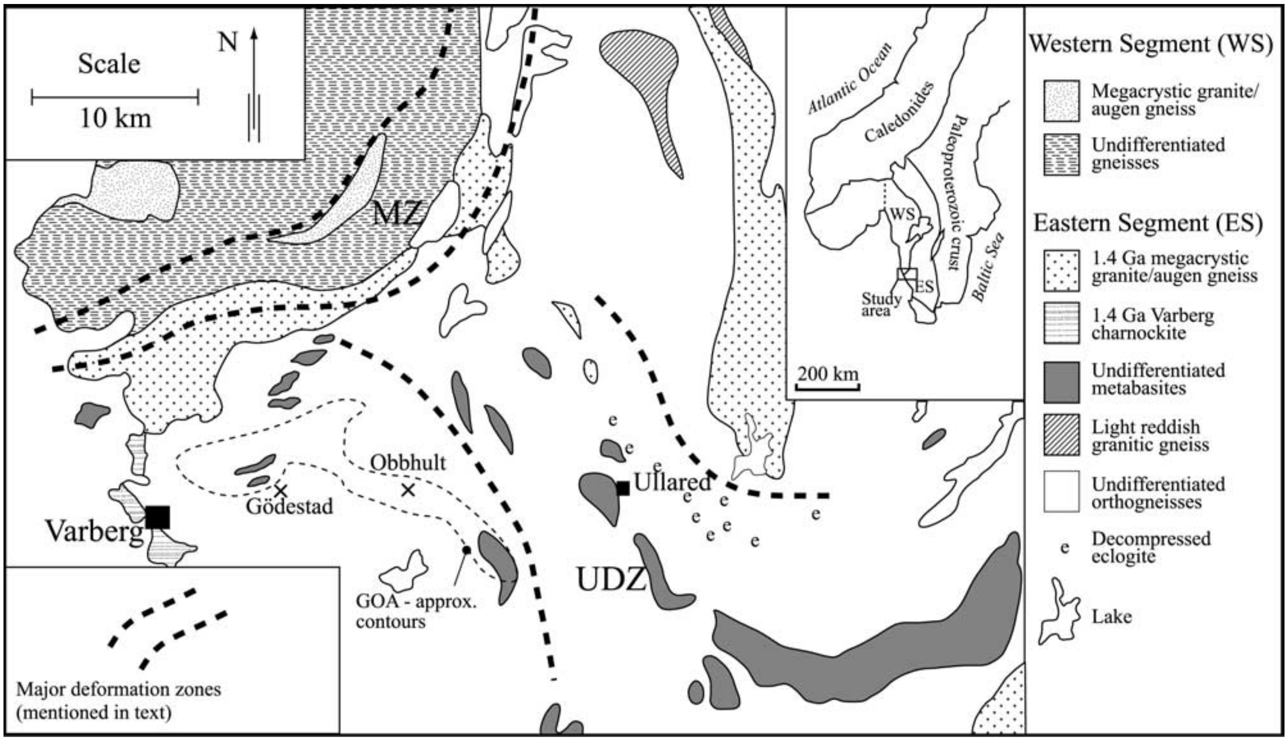

Figure 1. Geological map of the Varberg-Ullared area, modified from *Möller et al.* [1997, and references therein] (with permission from the author and Blackwell Publishing Group). Inset map illustrates the location of the eastern segment in the Sveconorwegian orogen, southern Scandinavia. Sveconorwegian orogenic units: ES, eastern segment; IT, Iddefjorden Terrane (western segment); K, Kongsberg region; B, Bamble Region; T, Telemark Region; R-A, Rogaland-Agder Region; TIB/SK, Transcandinavian Igneous Belt and the Svecokarelian Orogen. O, Oslo paleorift. Sveconorwegian deformation zones: PZ/SFDZ, Protogine Zone/Sveconorwegian Frontal Deformation Zone; MZ, mylonite zone; GOA, Gödestad-Obbhult Anomaly; e, decompressed eclogite; LA, lilla Ammås eclogite. Lakes: LV, Lake Vänern (northeast); Lake Vättern (southeast).

to the high paleomagnetic stability [*Merrill*, 1968; *Robinson et al.*, 2002; *Kasama et al.*, 2004; *McEnroe et al.*, 2004; *Harrison et al.*, 2006], and the present area is characterized by distinct negative aeromagnetic anomalies. Such anomalies might be ascribed to the presence of exsolved hematite-ilmenite, but they are also large-scale features that need a varied approach to be well described. Here, we present data from granulites sampled in or close to the same anomaly investigated by *McEnroe et al.* [2001], but instead of making detailed magnetic characterization and TEM investigations, we include paleomagnetic sites and mineralogical characterization of (1) rocks of varying bulk composition and (2) rocks with varying degree of retrogressive metamorphism.

[3] How can demagnetization and rock magnetic data be used for prediction of geomagnetic variations in the crust? This important question is put on its edge using the rock magnetic variation inherent in high-grade metamorphic rocks.

2. Regional Geology and Geochronology

[4] Currently different ways to subdivide the Precambrian of the southwestern Baltic shield exist (for review, see *Andersen* [2005]). Generally, these divisions in blocks or segments have been based on different metamorphic histories, on the occurrence of major deformation zones and on geochronological constraints. In this paper the domain bounded by the mylonite zone (MZ) to the west and the protogine zone in the east shall be called the eastern segment (ES). The MZ bends from a more N-S directed trend, which dominates further to the north, into an E-W directed lineament separating the two crustal blocks (Figure 1). The studied area is located in the ES. The ES consists mainly of Paleoproterozoic granites formed at circa 1.66–1.70 Ga, which were later deformed and migmatized at circa 1.44 Ga. At circa 0.97 Ga these gneisses underwent a second high-grade deformation and metamorphic event. This so-called Sveconorwegian event resulted in a new generation of migmatites and in the formation of granulites. The Sveconorwegian metamorphism was characterized by high pressure, leading to formation of kyanite-bearing high-pressure granulites. Eclogites were also formed. These eclogites were first recrystallized to high-pressure granulites during decompression, and later they were partly retrogressed to amphibolites [*Möller*, 1998].

[5] We investigated granulites in two areas ~20 km S-SW of the MZ. The places are called Gödestad and Obbhult (Figure 1). In Gödestad, there is a mafic granulite with minor compositional variation, but the degree of retrogres-

sive metamorphism to amphibolite varies, whereas in Obbhult there are granulites of different bulk composition. The ages of the protoliths of the Gödestad and Obbhult granulites are unknown. The metamorphic crystallization age of the rocks in Obbhult is assumed to be circa 1.4 Ga based on preliminary U-Pb dating of zircons (C. Möller, unpublished data, 2002). Of greater importance, however, are the ages of the later high-grade events and their subsequent uplift related cooling histories. As previously mentioned there is some evidence for metamorphism at 1.4 Ga in Obbhult, but because of the dependence of magnetic properties on temperature it is more relevant to consider the Sveconorwegian event. U-Pb datings of zircons from Obbhult gave ages around 970 Ma (C. Möller, unpublished data, 2002). This age is similar to that of the zircon inclusions in the eclogite garnets at Ammås near Ullared 10 km to the east of Obbhult (Figure 1) [*Johansson et al.*, 2001].

[6] *Page et al.* [1996] and *Wang et al.* [1998] reported ^{40}Ar-^{39}Ar datings of hornblende. Their studies suggest that this part of the ES cooled to temperatures below ~500°C at circa 930 Ma. There is no doubt that the crust was thickened regionally due to the Sveconorwegian event. ^{40}Ar-^{39}Ar datings of syntectonic hornblendes from the MZ consequently gave younger ages around 915 Ma, indicating later Sveconorwegian movements at amphibolite facies conditions along the MZ. Only one muscovite age at 904 Ma has been reported ~15 km to the ENE of Obbhult and Gödestad. In conclusion, cooling through the temperature range of interest for rock magnetic studies occurred at circa 0.93 Ga (500°C) with minor evidence of uplift at 904 Ma (350°C) (see *McDougall and Harrison* [1988] for closure of isotope systems).

3. Regional Geophysics

[7] We call the anomaly where we have conducted our study the Gödestad-Obbhult Anomaly (GOA) (Figure 2). The GOA consists of a nearly E-W trending slightly curved area with a negative anomaly in total field intensity. Figure 2 shows its extension together with profiles across the feature. The data are from the Geological Survey of Sweden. The minimum value of the anomaly is about −1500 nT, and it is bounded to the south and to the north by sharp gradients. The whole anomaly is ~5 km wide and 20 km long. The regional geomagnetic field is 40.054 A/m or 50 310 nT. Right north of the GOA there is a somewhat less defined and broader region with high total field intensity, containing small areas of sharp negative anomalies. In the north, this magnetic high area grades over successively to anomalies related to the MZ (or some counterpart to the MZ). Right south of the GOA there is also a positive anomaly, and to the east it is bounded by large-scale, N-S trending anomalies that may arise due to a deformation zone. To the SE, aeromagnetic anomalies are due to the Ullared Deformation Zone (UDZ) (Figures 1 and 2). The strongly negative total field intensities inside the GOA indicated that rocks with exceptional magnetic properties were present, and according to a previous study, rocks with high Q values existed in the vicinity of Gödestad near the town Varberg [*McEnroe et al.*, 2001] (Figure 2). In the middle of the GOA there is a jump in its east west trending borders. This might be the result of a fault that displaced the western part of the GOA to the north.

[8] The age of the regional uplift following the Sveconorwegian orogeny was circa 930 Ma according to ^{40}Ar-^{39}Ar datings of hornblende (section 2). One purpose here is to assess ages to those partial components, which could contribute to the anomaly. Later we shall make such comparisons using apparent polar wander path (APW) data from Baltica, and the related paleomagnetic literature. Examples of paleopoles with comparable ages are those of the Blekinge Dalarna Dolerite (BDD) dike swarm [*Söderlund et al.*, 2005] and the Egersund Ogna anorthosite complex in southern Norway (Table 1). The BDD lies west of the Protogine Zone (PZ) and that could indicate less Sveconorwegian resetting, but if they cooled quicker they should also have recorded more geomagnetic disturbances. The Egersund Ogna anorthosite paleopole is interpreted as due to uplift at circa 900 Ma, associated with formation of chemical remanent magnetizations (CRM) in exsolved hematite-ilmenite lamellae [*Brown and McEnroe*, 2004]. Somewhat older poles exist for the Laanila-Ristijärvi dikes, and the Kautokeino dikes at 1042 and 1062 Ma, respectively (both in Finland) [*Mertanen et al.*, 1996]. These dikes are even further away from Sveconorwegian influence compared to BDD. The Hunnedalen dikes in southwestern Norway are circa 855 Ma old [*Walderhaug et al.*, 1999], but that is a Sm-Nd whole rock age, which is less robust compared to U-Pb data, and the dikes sit in a terrane characterized by regional uplift/cooling. If one chooses the same polarity as *Bylund* [1992], all data needed for our specific interpretations will plot in the southern Pacific Ocean, however (plat 195°–270° and plong 10°–(−60°)). When interpreting the data with respect to their natural remanent magnetization (NRM) age, we will compare with this plot but we cannot yet determine an overall choice of polarity (paleomagnetic south or north poles).

4. Petrographical and Mineralogical Observations

[9] The rocks in Obbhult are complex with at least six different granulite types. They occur in parallel slabs (read discs) of different thicknesses, each characterized by a characteristic composition and degree of veining/metamorphic differentiation. We thus sampled all these slabs, that we from now on call OBB L1–OBB L6. During description of the magnetic data we will refer to samples from these layers as the paleomagnetic sites OBB 1–OBB 6, and in the site OBB 2 an extra site named OBB 2B was sampled in order to use for extra checks of magnetometer intensity data. OBB L1 is ~10 m thick, OBB L2 ~10 m, OBB L3 ~5 m, OBB L4 ~5 m, OBB L5 ~20m, and OBB L6 is ~30 m thick. Since the rocks are intensely metamorphosed it is presently impossible to determine their protoliths. The differences between the units are distinct. Deformation may not always show up as foliation on the grain size scale, but it is obvious due to the much larger structures (the occurrence of distinct layers). Grain boundaries in between the silicate minerals are equilibrated and angular to rounded, which makes these loose and grainy. Veins with scapolite and minor sulphides occur. Typical of OBB L6 is the occurrence of veins of

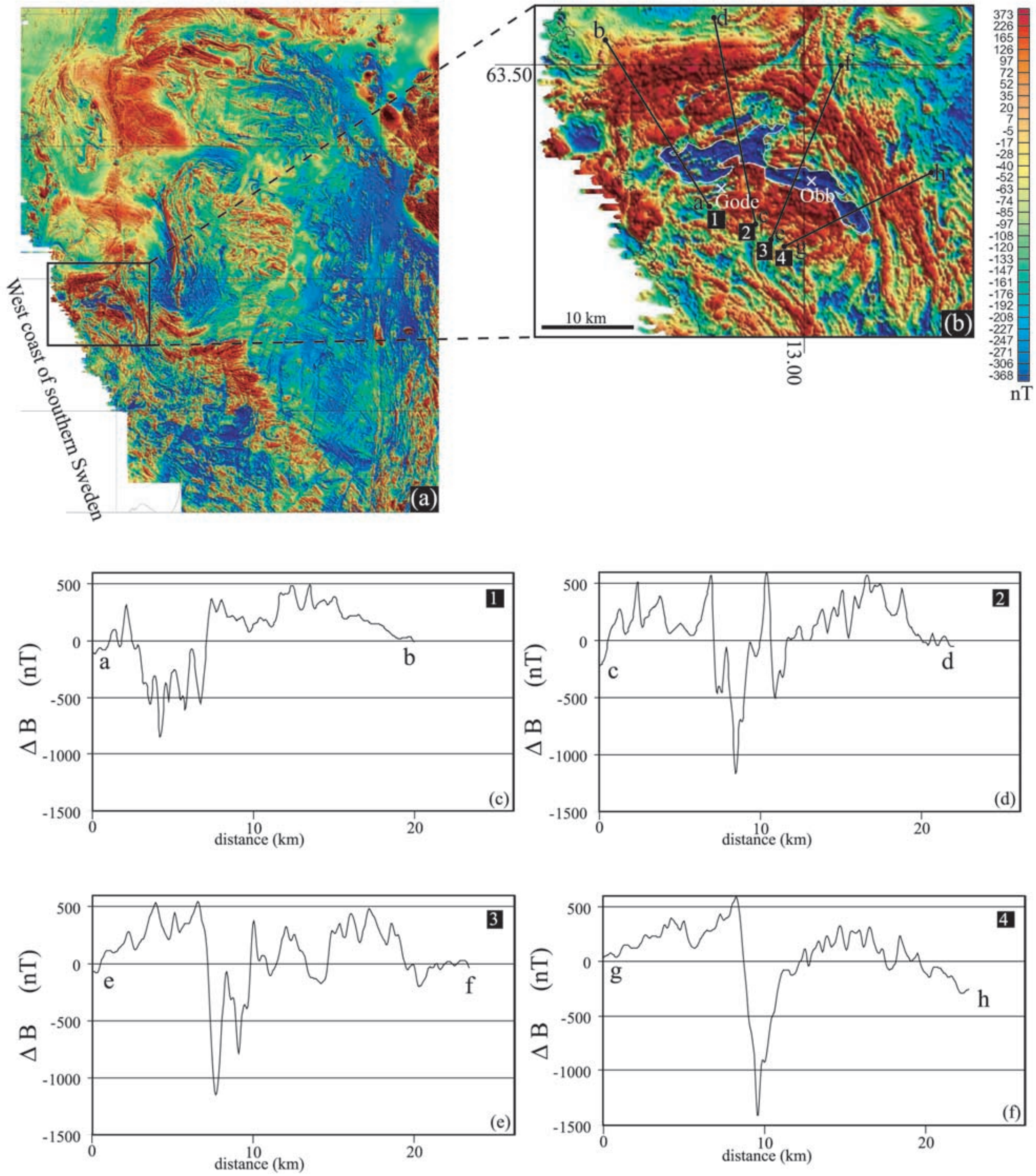

Figure 2. Aeromagnetic maps and profiles with total geomagnetic field intensity in the investigated area. (a) Regional aeromagnetic map, approximately over the same area as in Figure 1. (b) Aeromagnetic map over the area around the GOA. (c–f) Profiles with total geomagnetic field intensity across the GOA. The locations of these profiles, which are denoted 1–4, are shown in Figure 2b. Data are from the Geological Survey of Sweden, airborne magnetic measurements (© Sveriges Geologiska Undersökning (SGU), permission 30-1342/2006).

Table 1. Paleopoles From Baltica From the Time Interval 550–1271 Ma

Rock Formation	Age	plat	plong	D_p	D_m	Reference
Winter Coast red sedimentary rocks[a]	550	−24	132	2.3	3.8	*Popov et al.* [2002]
Sredniy-Kildin red beds[a]	750–535	30	196	6	12	*Shipunov and Chumakov* [1991]
Vadsö Group B[a]	750–535	23	209	4.5	9	*Bylund* [1994]
Kildinskaya Formation HB[b]	750–535	25.5	193.1	4	7	*Torsvik et al.* [1995]
Visingsö beds[a]	735	−7	256	8	13	*Lewandowski et al.* [2004]
Hunnedalen dikes[a]	855, 848	−41	222	10	11	*Walderhaug et al.* [1999]
Tärnö Dolerite[b]	871	−0.3	237	3.6	5.9	*Patchett and Bylund* [1977]
Egersund Ogna Anortosit[a]	900–950	−42.1	200.4	9	9.4	*Brown and McEnroe* [2004]
Obbhult[a]	circa 930	−24	218	9.4	9.9	this paper
Gödestad[b]	circa 930	−51	203	4.4	5.6	this paper
Lösen Fäjö[b]	946	−23	249	2.7	5.4	*Patchett and Bylund* [1977]
Falun Dolerite[b]	946	−6.1	237.6	4.6	7.1	*Patchett and Bylund* [1977]
Bräkne Hoby[b]	949	−22	252	3.1	6.1	*Patchett and Bylund* [1977]
Karlshamn Dolerite[b]	954	−40	207	4	4	*Patchett and Bylund* [1977]
Bo Dolerite[b]	950–1560	−4	244	10	17	*Piper* [1980]
Nilstorp Dolerite[b]	966	9	239	5.8	11	*Patchett and Bylund* [1977]
Årby Dolerite[b]	995	−7.3	227.4	6.8	9.5	*Patchett and Bylund* [1977]
Laanila-Ristijärvi dikes[b]	1042, 1013	−2	212	13	21	*Mertanen et al.* [1996]
Kautokeino dikes[b]	1062	−35	237	3.1	5.4	*Mertanen et al.* [1996]
Märket Dolerite dikes[a]	1265	−6	146	6.7	11	*Neuvonen and Grundström* [1969]
Saatakunta Dolerite dikes and sills[a]	1264	2	158	2.4	4.4	*Buchan et al.* [2000]
Vaasa Dolerite dikes[a]	1268	7	164	3.2	5.5	*Neuvonen* [1966]
CSDG mean (Jämtland, Sweden)[a]	1264–1271	0.6	161	6.3	11	*Elming and Mattsson* [2001]

[a]The data were based on a number of sites.
[b]The data were based on a number of samples.

coarse plagioclase, clinopyroxene and brown orthopyroxene. Possibly these have formed during partial melting.

4.1. Obbhult, Layers 1–6

4.1.1. OBB L1

[10] OBB L1 is a lightly colored rock layer, consisting mainly of plagioclase quartz and orthopyroxene (see Figures 3a and 3b). The plagioclase is partly recrystallized to a more fine-grained mosaic of plagioclase with straight grain boundaries. There is no compositional difference between the two modes of occurrence. The composition of the plagioclase is approximately $Ab_{70}An_{30}$. The orthopyroxene forms up to centimeter-sized megacrysts in a matrix of plagioclase and quartz, and it is rusty brown due to very fine numerous exsolution-lamellae. These lamellae could not be analyzed with microprobe analyses because of the small sizes, but they were rich in titanium. The opaque minerals form irregular shaped millimeter sized grains and they consist of hematite with exsolution lamellas of ilmenite. Corundum occurs sparsely within the exsolved ilmenite. Corundum grains were surrounded by ilmenite rims, and zircon is a common accessory mineral.

4.1.2. OBB L2

[11] This slab consists of recrystallized plagioclase, biotite, garnet, orthopyroxene and oxides. Apatite is a common accessory mineral. Most opaque grains consist of hematite with numerous very thin exsolution lamellas of ilmenite and they are in the size range 200–500 μm, but some may be up to 3 mm in size.

4.1.3. OBB L3

[12] This rock consists of fine-grained ($\sim$0.1 mm) plagioclase biotite and clinopyroxene. Minor amounts of amphibole occur. Little clinopyroxene occur and seems to coexist with amphibole. Occasionally amphibole dominates over clinopyroxene. Orthopyroxene occurs as an accessory mineral. The rock is foliated and granoblastic. In this layer there are approximately equal amounts of magnetite and hematite. Most of the hematite lack exsolution lamellae, at least on the scale >0.1 μm. Some hematite grains have very thin and short ($\sim$10 μm long) exsolution lamellae of ilmenite. The magnetite has been partly oxidized to hematite. That is a volumetrically subordinate phenomenon and it is mainly seen along small fractures in the magnetite. Most magnetite and hematite grains are 50–200 μm but some magnetite grains may be up to 1000 μm.

4.1.4. OBB L4

[13] This slab consists mainly of coarse-grained perthitic feldspar biotite and opaques. Some opaques are associated with corundum occurring in certain metamorphic textures. Small grains of bluish sapphirine are associated with the oxides. In this layer magnetite is far more common than hematite. The relative amounts are estimated to $\sim$75% and 25%, respectively. The grain size of the magnetite is in the range 50–1000 μm with most grains >500 μm. Magnetite and hematite often form larger composite grains without any signs of reaction along their grain boundaries. The hematite lacks exsolved ilmenite-lamellae.

4.1.5. OBB L5

[14] Plagioclase occurs as small granoblastic grains. The feldspar also occurs as coarser perthites and biotite and garnet are abundant. Corundum garnet and fine-grained oxides occur in elongated few millimeter wide patterns. Sapphirine is also common here. With respect to the oxide mineralogy this is the most complex rock type. Hematite with thin ilmenite exsolution-lamellae occurs as single 200–500 μm sized grains, but also in symplectites intergrown with the silicates. A third textural variety of opaque minerals consist of minute oxide plates along two distinct crystallographic planes in the sapphirine. Because of their small sizes they were impossible to analyze with microprobe. From our observations in reflective light, it was clear that there were two different minerals resembling hematite

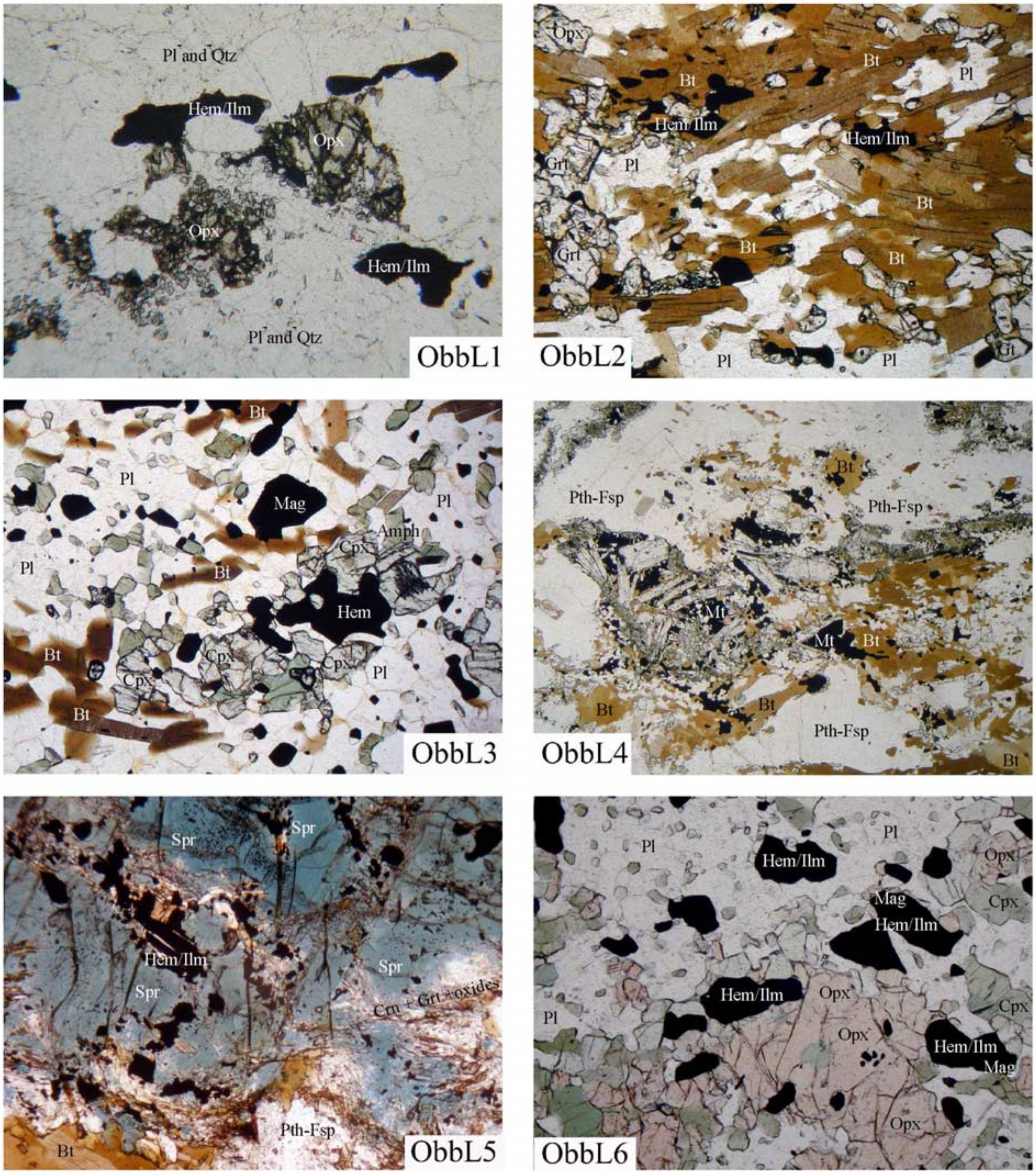

Figure 3a. Photomicrographs of representative samples from sites OBB L1 to OBB L6. The widths of the photos are 4 mm for OBB L1, OBB L2, and OBB L3; 2 mm for OBB L5 and OBB L6; and 8 mm for OBB L4. For descriptions of the mineralogy, see section 4. Abbreviations follow *Kretz* [1983] except for Pth-Fsp, perthitic feldspar, and Amph, amphibole.

and magnetite. Beside this possible occurrence in sapphirine, no magnetite was identified in OBB L5.

4.1.6. OBB L6

[15] This slab consists of a mafic rock with varying degrees of metamorphism. Orthopyroxene plagioclase and biotite were observed along with symplectites, which have formed during garnet decomposition. Two oxide associations occur, single larger grains, and finer grains associated with the symplectites. Occasionally there is plagioclase clinopyroxene orthopyroxene and amphibole in approximately equal amounts. No garnet grains or symplectitic textures were associated to the later. The magnetite and hematite form composite grains some of which are up to 2 mm in size. There are relatively few (>10 μm sized)

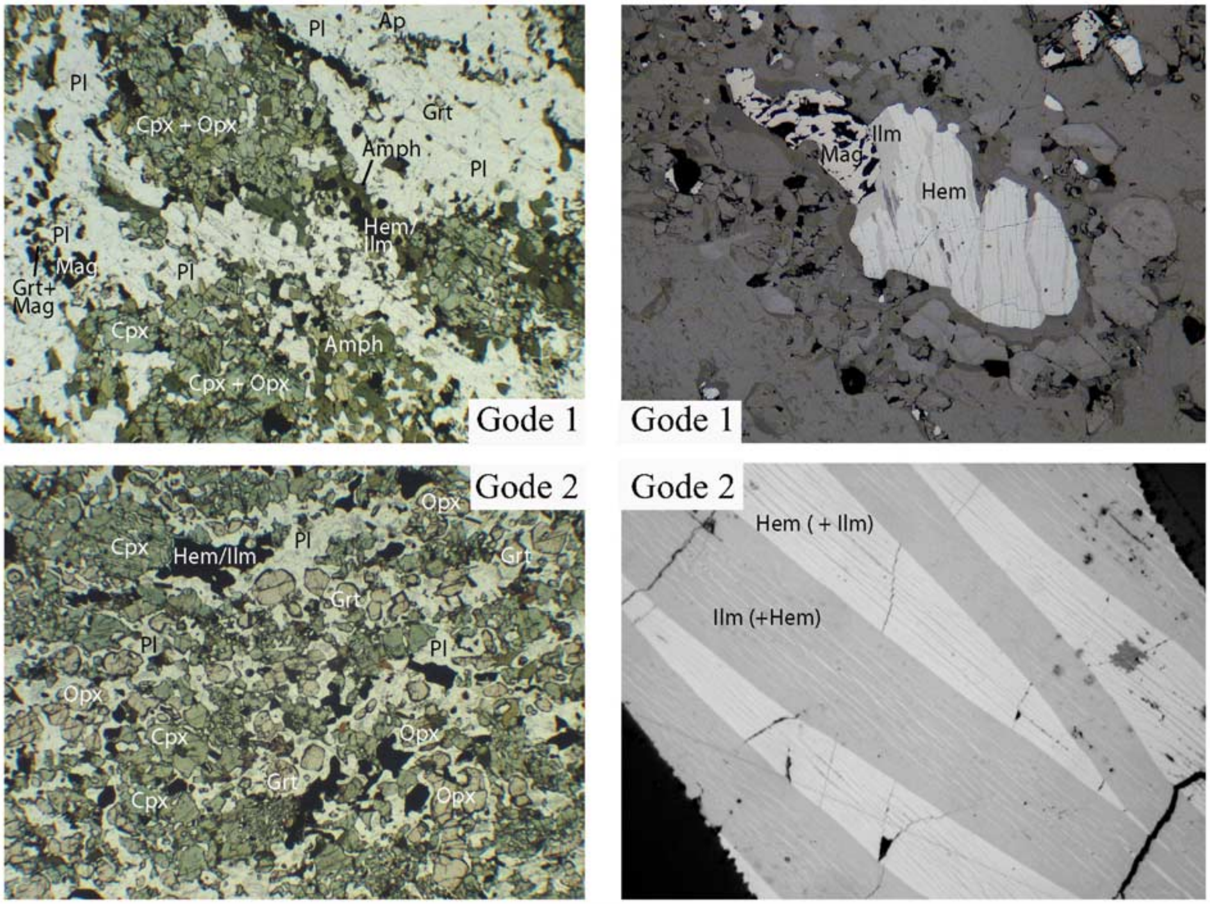

Figure 3b. Photomicrographs of representative samples from sites GODE 1 and GODE 2. (top right) A composite magnetite-hematite grain. These types of composite grains were common in GODE 1, but they were not found in the GODE 2 samples. (bottom right) The complex exsolution relationships between hematite (light grey) and ilmenite (dark grey). The widths are 4 mm for Figure 3b (left), 1.65 mm Figure 3b (top right), and 0.175 mm Figure 3b (bottom right). Abbreviations according to *Kretz* [1983] except Amph, amphibole.

exsolution-lamellae of ilmenite in the hematite, and they are clearly more common near grain boundaries toward the magnetite (Figure 4). The magnetite is associated with the hematite, and no solitary magnetite grains occur. In most of the hematite there are no exsolution textures visible in optical microscope. However, this is a false impression since scanning electron microscopy clearly shows extremely fine (<200 nm) exsolution textures in the hematite (Figure 4).

4.2. Gödestad Samples

[16] At the nearby Gödestad locality (Figure 3b) we have distinguished two types of mafic granulites, each characterized by different degrees of alteration to amphibolite. We sampled these varieties from now on called GODE 1 and GODE 2. No contacts between the GODE 1 and GODE 2 types were visible in the field, but they represent a gradual transition observed between adjacent outcrops.

4.2.1. GODE 1

[17] This rock is even-grained and foliated, and it consists of plagioclase, clinopyroxene, orthopyroxene, garnet, amphibole and minor biotite, apatite, scapolite and pyrite. The oxides consist of hematite with exsolution lamellae and of magnetite. Their grain sizes range from 50 to 250 μm, but single magnetite grains may be up to 1.5 mm. There are approximately equal amounts of hematite/ilmenite and magnetite in the samples, but there is a large variation in the relative amounts between them.

4.2.2. GODE 2

[18] In this rock the retrograde reactions were less important. It consists mainly of plagioclase clinopyroxene orthopyroxene, and garnet. Minor amounts of apatite biotite and hornblende occur. The opaque mineral is hematite with exsolved ilmenite. The exsolution textures are more complex due to the occurrence exsolved lamellae, but inside the previously formed ilmenite-lamellae (Figure 3b).

5. Sampling, Measurements, and Methodology

[19] We drilled seven sites in Obbhult and two sites in Gödestad. In Obbhult, the seven sites represent the six granulite varieties described under (4), together with an extra site in the unit OBB L2, sampled in order to inves-

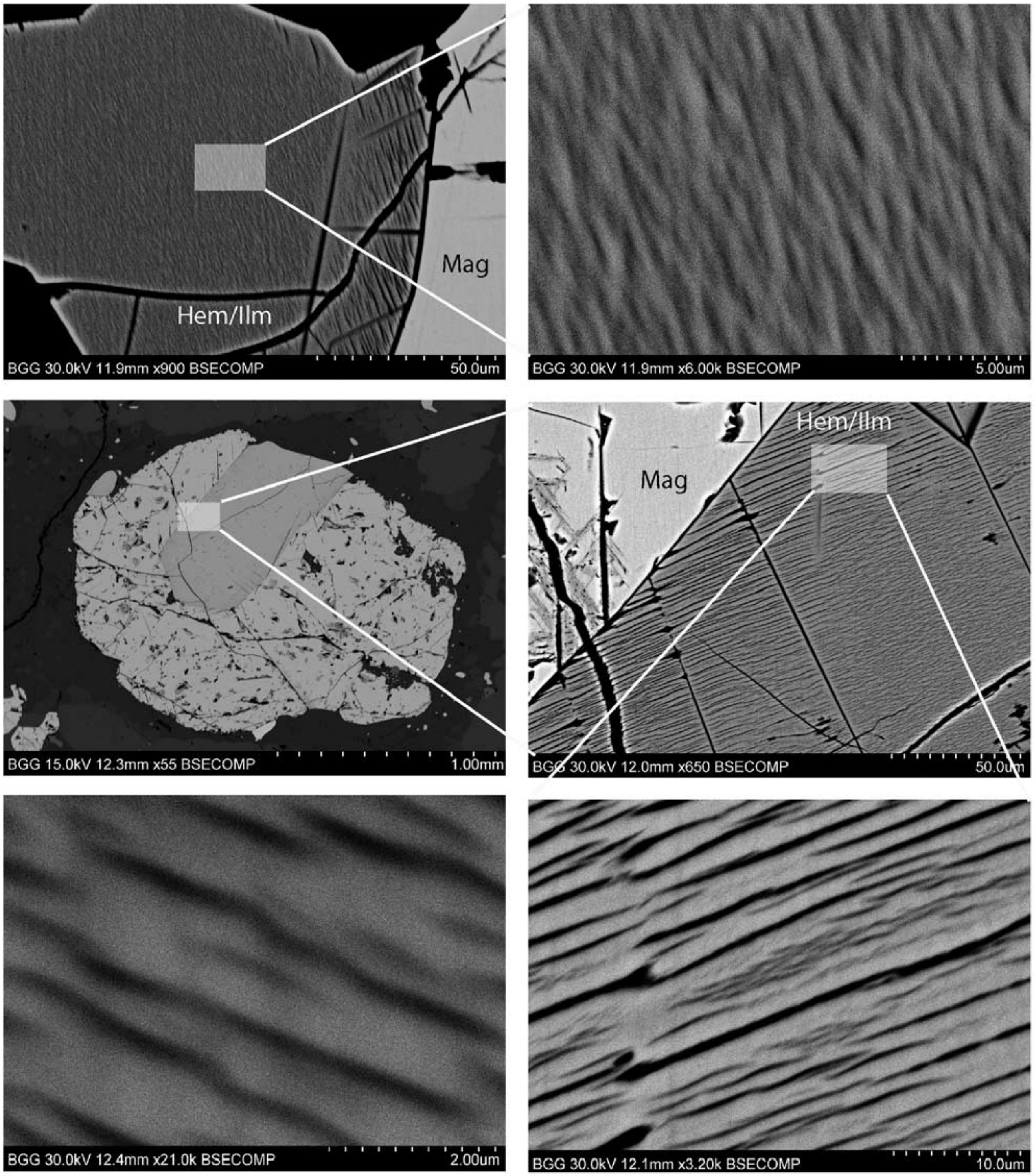

Figure 4. Electron micrographs of typical hematite-ilmenite exsolution relationships in OBB L6. Similar textures were common also in layers OBB L1, OBB L2, and OBB L5. Figure 4 (bottom left) show very thin exsolution lamellas (<200 nm). Note that these lamellae were coarser close to the hematite-magnetite grain boundary. In the interior of the hematite the exsolution lamellas are shorter, much smaller, and irregularly shaped. This is clearly seen in Figure 4 (middle right).

tigate the usage of two different magnetometers (OBB 2). In Gödestad they represent two granulite varieties with different degree of metamorphic retrogression (4). The rock magnetic sites are called OBB 1–OBB 6, OBB 2B and GODE 1 and GODE 2, respectively. The drill cores were split in two parts before demagnetization, one for thermal and one for alternating field (AF) demagnetization. The rock chips used for thin sections were also taken from these cores. The demagnetization was carried out in the Paleomagnetic Laboratory at Lund University, Sweden. The samples for AF demagnetization were demagnetized and their magnetization measured after exposure to alternating fields of 0, 10.. 50 mT and then continuing to 70, 90.. 150 mT. During AF demagnetization, the same field was applied in the x, y, and z directions of the sample coordinate system. The measurements were made with a 2G-Enterprises superconducting rock magnetometer model 755 R except for the OBB 2B site whose samples were measured with a Molspin Fluxgate magnetometer. The purpose of making the OBB 2B site was that this rock unit contained strongly magnetic samples giving to low intensities when measured with a 2G-SQUID. Site OBB 2 could not be used to determine NRM intensities, but demagnetization curve parameters according to paragraph 5.1 were calculated, and mean directions. Thermal demagnetization was made with a Magnetic Measurements Thermal Demagnetization oven (MMTD 80) in an outer field of less than 10 nT. During thermal demagnetization, χ was continuously measured with a Bartington susceptibility bridge in order to look for mineralogical reactions possibly induced by the heating. We measured χ with a Kappabridge KLY 2 (Geofyzika Brno), and the resultant values were used to calculate Koenigsberger ratios using a value for the regional geomagnetic field at 40 A/m. The measurements were made on both parts of the separated cores, and all values included in mean calculations. Weak field susceptibility was measured in air in the temperature interval $-196°$ to $700°C$ using the Kappabridge KLY 2, equipped with either a cryostat or a high-temperature furnace. In both cases, corrections were applied to subtract the susceptibility dependencies of these.

5.1. Statistical Treatment and Calculations

[20] In order to quantitatively compare demagnetization behavior of our sites (and in the future with other sites) we must solve the problem of giving numerical values, to describe the rows of small vectors that constitute the demagnetization curves. Our method has similarities to *Petrova* [1961], *Ade-Hall* [1969], and E. Eneroth (Palaeomagnetic unblocking data as indicators of the micromagnetic state in magnetite: Implications for palaeomagnetism?, manuscript in preparation 2007). It is merely a tool adjusted to modern demagnetization practices. In Figure 5, we have defined the symbols NRM, RM_k, $\mathbf{v}_k$, $\mathbf{c}_k$ and $\mathbf{r}$. They denote the following vectors: NRM is the natural remanent magnetization vector, RM_k is the residual magnetization vector at demagnetization step k, $\mathbf{v}_k$ is a minor vector component demagnetized at demagnetization step k, if it is not part of the characteristic remanent magnetization (ChRM), $\mathbf{c}_k$ is such a minor component if it is contained in the ChRM, and $\mathbf{r}$ is the residual magnetization vector after the demagnetization was completed. Now we define the following experimental and rock magnetic parameters:

$$L = \frac{|\mathbf{NRM}|}{\sum_{\mathbf{k}} |\mathbf{c_k}| + \sum_{\mathbf{k}} |\mathbf{v_k}| + |\mathbf{r}|} \qquad (1)$$

We hereby call this entity L because it is equal to one if the demagnetization curve is perfectly linear. Bent or noisy curves will give lower L. In equation (1) the denominator is identical to the vector difference sum of *Tauxe* [1998]:

$$F_r = \frac{|\mathbf{r}|}{\sum_{\mathbf{k}} |\mathbf{c_k}| + \sum_{\mathbf{k}} |\mathbf{v_k}| + |\mathbf{r}|} \qquad (2)$$

We choose to call this entity F_r because it represents the residual magnetization after completed demagnetization, calculated as a fraction of all demagnetized partial components (L values might be irrelevant if F_r is larger than 0.2):

$$F_{ch} = \frac{\sum_{\mathbf{k}} |\mathbf{c_k}|}{\sum_{\mathbf{k}} |\mathbf{c_k}| + \sum_{\mathbf{k}} |\mathbf{v_k}| + |\mathbf{r}|} \qquad (3)$$

We hereby call this F_{ch} because it depends on the total length of all demagnetization components included in the "ChRM," calculated as a fraction of all that was demagnetized. L, F_r and F_{ch} contain information about the shapes of demagnetization curves, and if mean angular deviation (MAD) values for ChRM also are given the description will be better, because reduced L due to noisy curves might be distinguished from reduced L due to bent curves. L, F_r and F_{ch}, shall also be indexed with th and af in the following to separate thermal from AF demagnetization. So far, we have only considered the purely geometrical properties of the curves and not their unblocking spectra. In order to do this, we now define H_{c25}, H_{c50}, H_{c75}, T_{ub25}, T_{ub50} and T_{ub75}, and doing this, we first consider the summed lengths of the residual magnetization components at any demagnetization step (for instance, a temperature). This length may be either less or more than 75% of the denominator in equations (1)–(3). If less, then the T_{ub75} value is found by linear interpolation between that temperature, and the preceding demagnetization temperature (which should represent a step with summed length of more than 75% of the denominator in equations (1)–(3)). In analogy with this, we can also define the other parameters both for AF and thermal demagnetization, but then we use 50 and 25% instead of 75%. We call this way to calculate unblocking spectra, method A. Method B is to consider 75, 50 or 25% of the initial intensity, and use linear interpolation between points in the raw data curves (decaying intensity curve) in order to see where the decay curve crosses this value. Method B should be used when there is noisy unstable demagnetization behavior or spurious acquisition of components at high temperatures. If we used method A on such samples we would get meaninglessly high T_{ub} values.

[21] We have performed these calculations on our thermally demagnetized samples with few exceptions. Because of high coercivities, the calculations were not possible when using AF demagnetization results, except for units OBB 3 and OBB 4. For the samples that were impossible to demagnetize with AF we give F_r only and not the other parameters. During calculation of H_{c25}, H_{c50}, and H_{c75} for sites OBB 3 and OBB 4 we did not include $\mathbf{r}$ in the denominator of equations (1)–(3). This was due to a relatively high and stable $\mathbf{r}$ component, which seemed physically unrelated to the major components of interest. We have also given the upper and lower limits used during

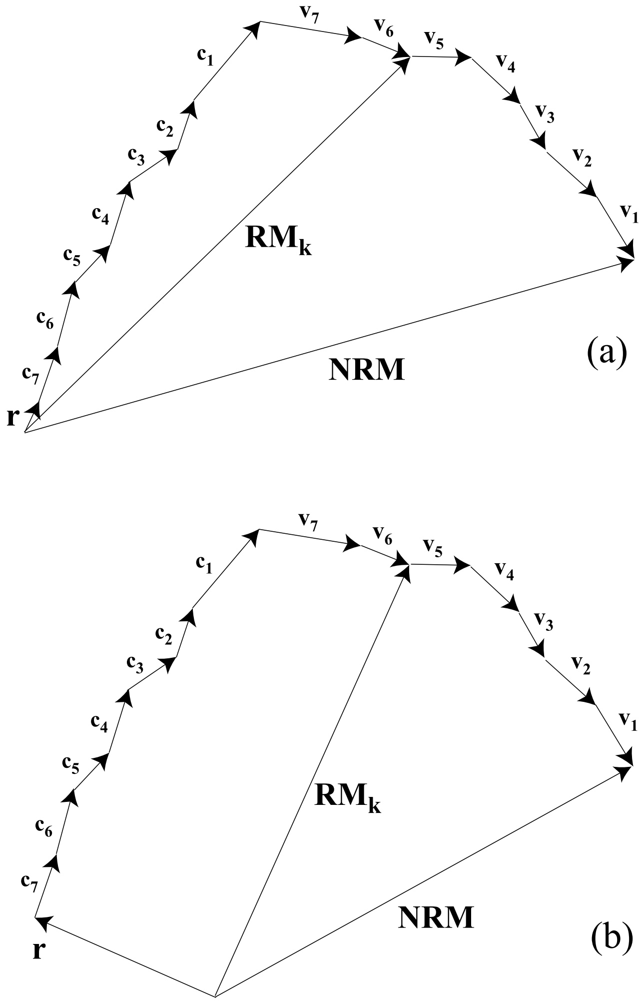

Figure 5. Symbolic illustration of demagnetization projected in two dimensions together with names of the minor vector components used in equations (1)–(3). (a) A case of type 1 in section 5, where the residual component is assumed to be closely related to the ChRM and is minor. (b) A case of type 2 in section 5 where the residual component is large and has another direction than the ChRM.

principal component analysis (PCA) for AF and thermal demagnetization as AF1, AF2, TH1, and TH2, respectively, and standard deviations for these parameters. NRM intensities were calculated in two different ways. First, by ordinary arithmetic means, and second by adding vectors instead of scalars during the calculation:

$$\langle \mathbf{NRM} \rangle = \frac{\sum_{k=1}^{m} \mathbf{NRM}_k}{m} \quad (4)$$

The calculation of characteristic remanent magnetization ChRM directions and mean angular deviation (MAD) values for ChRM components were made with PCA in the Super IAPD program (http://www.geodynamics.no). Last, we calculated statistics according to *Fisher* [1953] for the ChRM components (dec/inc, k, α95 and R), and paleopoles and VGPs were calculated with Super IAPD (paleopole will be used for data based on one or more site mean directions and VGPs for data based on a number of samples).

[22] Before using these parameters to discuss our results we need to mention some possible complications. It is a common case that the ChRM represents a high-blocking component in the demagnetization curve, and that it might be related to **r**. If it is difficult to demagnetize a sample (for instance, when the AF fields are insufficient) it is necessary to distinguish two cases: (1) **r** is parallel to the ChRM, whereby it is assumed that it from a genetic point of view represents the most high blocking ChRM fraction and (2) **r** is either not parallel to the ChRM or somehow separated from it with respect to unblocking interval (Figure 5). A high F_r value, say 0.2, combined with case 2 is one of the cases that could make L a less trustworthy indication of the quality of the demagnetization result. For instance, in the case of two distinctly different magnetic carriers with different coercivities and responses to remagnetization events, a perfectly linear and stable ChRM component could end at a point whose trend toward the origin is not parallel with the ChRM (residing in the high-coercivity phase). Then a parameter such as L, could describe mixed phenomena without geological meaning. There could be a lower L value when compared to samples with truly unstable demagnetization of ChRM. As we shall see later, it could also be important to mind high F_r values and cases 1 and 2 when the coercive force and thermal unblocking spectra are calculated. It is important to mind another limitation due to method A, namely, the problem caused by noisy behavior (meaning that each demagnetized component is much inclined relative to the preceding step). This could give spurious high F_{ch} values when compared to L. In the future, it is of interest to make more tests to define criteria for the exclusion of F_{ch} from a data report. Such criteria must be based on MAD values.

6. Results From Paleomagnetic/Rock Magnetic Investigations

6.1. Demagnetization Results

[23] Typical examples of demagnetization raw data are shown in the Zijderveld diagrams in Figure 6, and as intensity curves in Figures 7 and 8. We now start this paragraph with a description of the OBB 1–OBB 6 sites. All samples from units OBB 1, OBB 2, OBB 5 and OBB 6 had N-NW directed declinations and steep negative inclinations (Figure 9). During AF demagnetization of the samples from units OBB 1, OBB 2, OBB 5, and OBB 6 the intensities were constant, so they have F_r values of 0.91–0.95 (Table 2, see also Figure 7, down to 0.82 when measured with Molspin OBB 2B). The parameters L F_{ch}

Figure 6. Alternating field (af) and thermal demagnetization (th) behavior of samples from Obbhult and Gödestad in Zijderveld projections. Open squares denote vertical projections and solid denote horizontal projections. (a–b) Site OBB 1, (c–d) site OBB 6, (e–f) site OBB 3, (g–h) site GODE 1, and (i–j) site GODE 2.

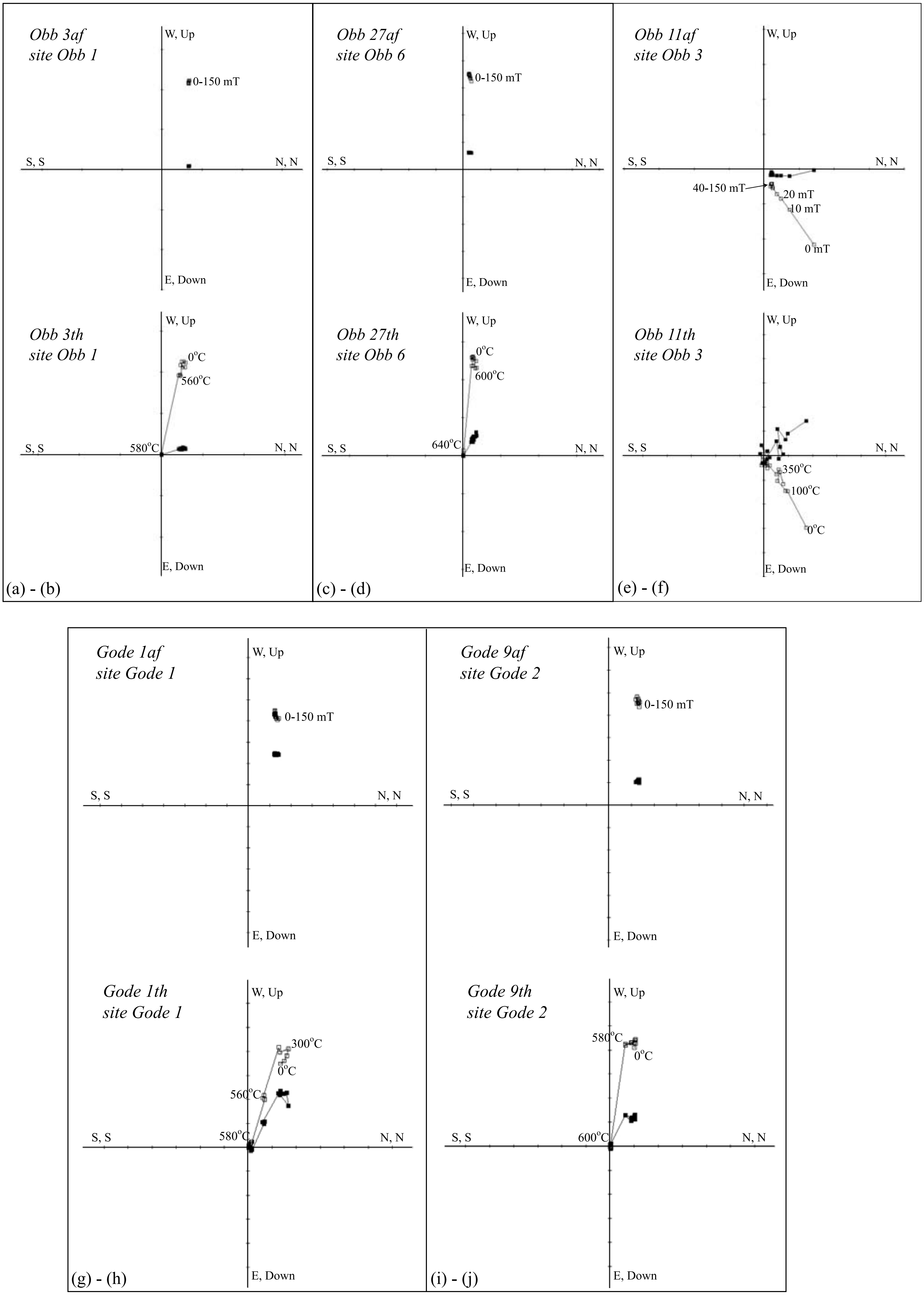
Obb 3af
site Obb 1
W, Up
0-150 mT
S, S
N, N
E, Down
Obb 3th
site Obb 1
0°C
560°C
580°C
(a) - (b)
Obb 27af
site Obb 6
0-150 mT
Obb 27th
site Obb 6
0°C
600°C
640°C
(c) - (d)
Obb 11af
site Obb 3
40-150 mT
20 mT
10 mT
0 mT
Obb 11th
site Obb 3
350°C
100°C
0°C
(e) - (f)
Gode 1af
site Gode 1
0-150 mT
Gode 1th
site Gode 1
300°C
0°C
560°C
580°C
(g) - (h)
Gode 9af
site Gode 2
0-150 mT
Gode 9th
site Gode 2
580°C
0°C
600°C
(i) - (j)

Figure 6

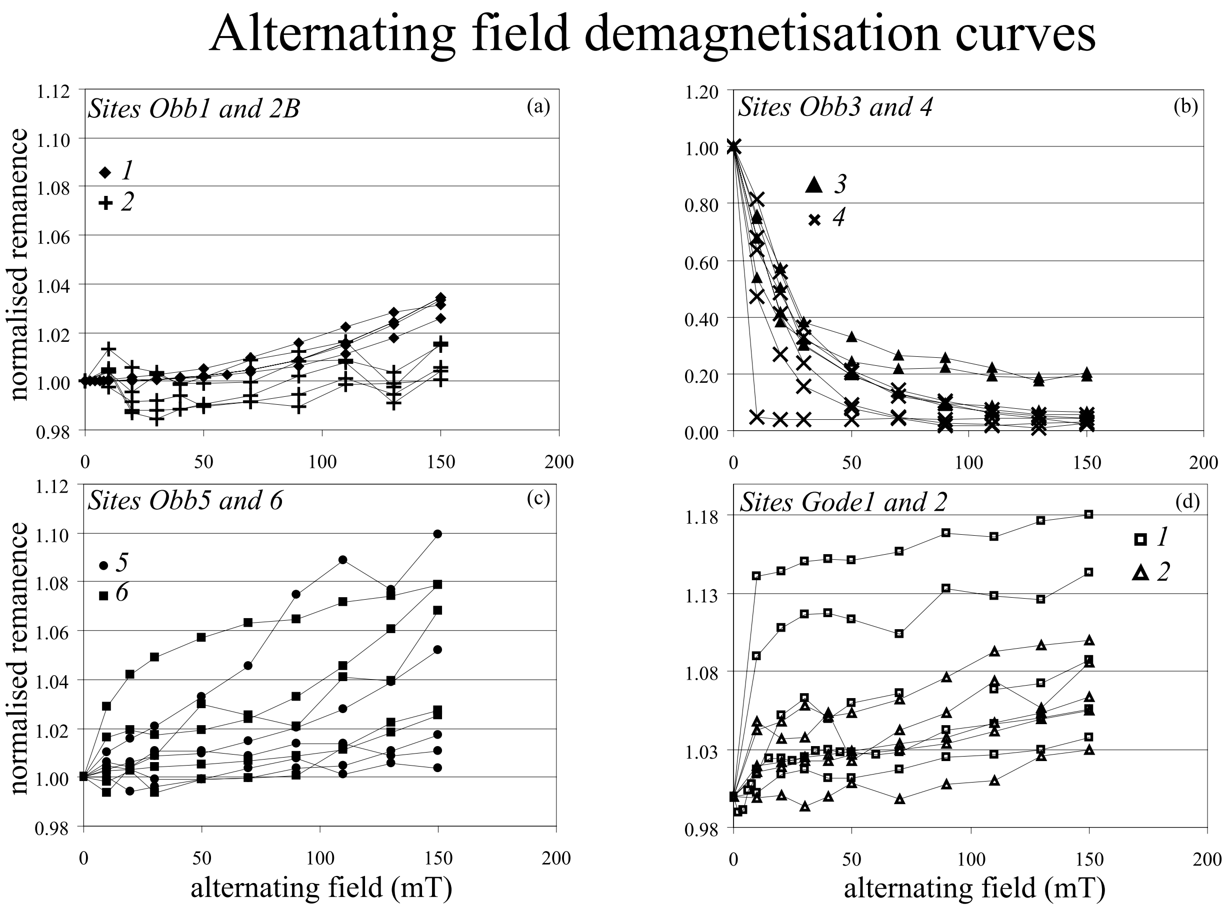

Figure 7. Remanent intensity as a function of alternating field during demagnetization. The curves were normalized with the initial values before plotting. (a) Results from the sites OBB 1 and OBB 2. (b) Results from the sites OBB 3 and OBB 4. (c) Results from the sites OBB 5 and OBB 6. (d) Results from the sites GODE 1 and GODE 2. Please note that the scale is expanded around the value one in Figures 7a, 7c, and 7d.

and MAD were of course not calculated for these samples. This also means that the directions plotted in Figures 9a–9c not are components calculated with PCA, but instead mean values estimated from dec/inc tables. They may differ from the NRM direction with ~3° at maximum. Note that the scale is expanded and centered around the value one in Figures 7a, 7c and 7d. Upon thermal demagnetization of samples from the same sites (OBB 1, OBB 2B, OBB 5, and OBB 6) there were sharply decreasing magnetizations in the interval between 560 and 610°C. Some samples from OBB 1 had decreases starting at lower temperatures. This follows from the T_{ub25} value of 541°C, which is lower than the other sites with this characteristic demagnetization behavior (Table 2 and Figure 10). The thermal demagnetization typically ended with F_r values at 0.002–0.02. L values were in the interval 0.69–0.77, F_{chth} were in between 0.72 and 0.79 and MAD were in between 0.90° and 1.90° (in Table 2, mean values are given, intervals were not regarded as relevant). For the sites OBB 5 and OBB 6 higher F_{chth} compared to the L values occurred. This was associated with demagnetization of a partial component below 400°C which was opposite in direction to the main component used for ChRM calculation (Figure 9e and Table 3).

[24] Samples from units OBB 3 and OBB 4 behaved much differently during both AF and thermal demagnetization. During AF demagnetization, the samples from OBB 3 decreased rapidly at AF fields of 0–50 mT, but in two of the samples, this decrease leveled out completely giving rise to F_r values around 0.2. The NRM of the OBB 4 samples had even lower coercivity, and the L values from AF demagnetization were 0.88 and 0.89 for sites OBB 3 and OBB 4, respectively. During thermal demagnetization the sites gave noisy data with MAD values of 15° and 7.0° clearly demonstrating their more unstable behavior during demagnetization (Figure 6). The L values from thermal demagnetization of OBB 3 and OBB 4 were 0.37 and 0.24 which is low. This type of instability made the samples unsuitable for calculation of F_{chth}. The values of F_{chth} would become much higher than the L values due to addition of the lengths of vectors inclined at large angles relative to each other, and a meaninglessly high F_{chth} would thus result. Because of unstable demagnetization we also calculated T_{ub} values with method B for the sites OBB 3 and OBB 4. In Figure 10 these T_{ub} values are seen. There is considerable lowering of T_{ub25} and T_{ub50} for OBB 3 and OBB 4 when compared to all the other sites, particularly when the B method values are considered.

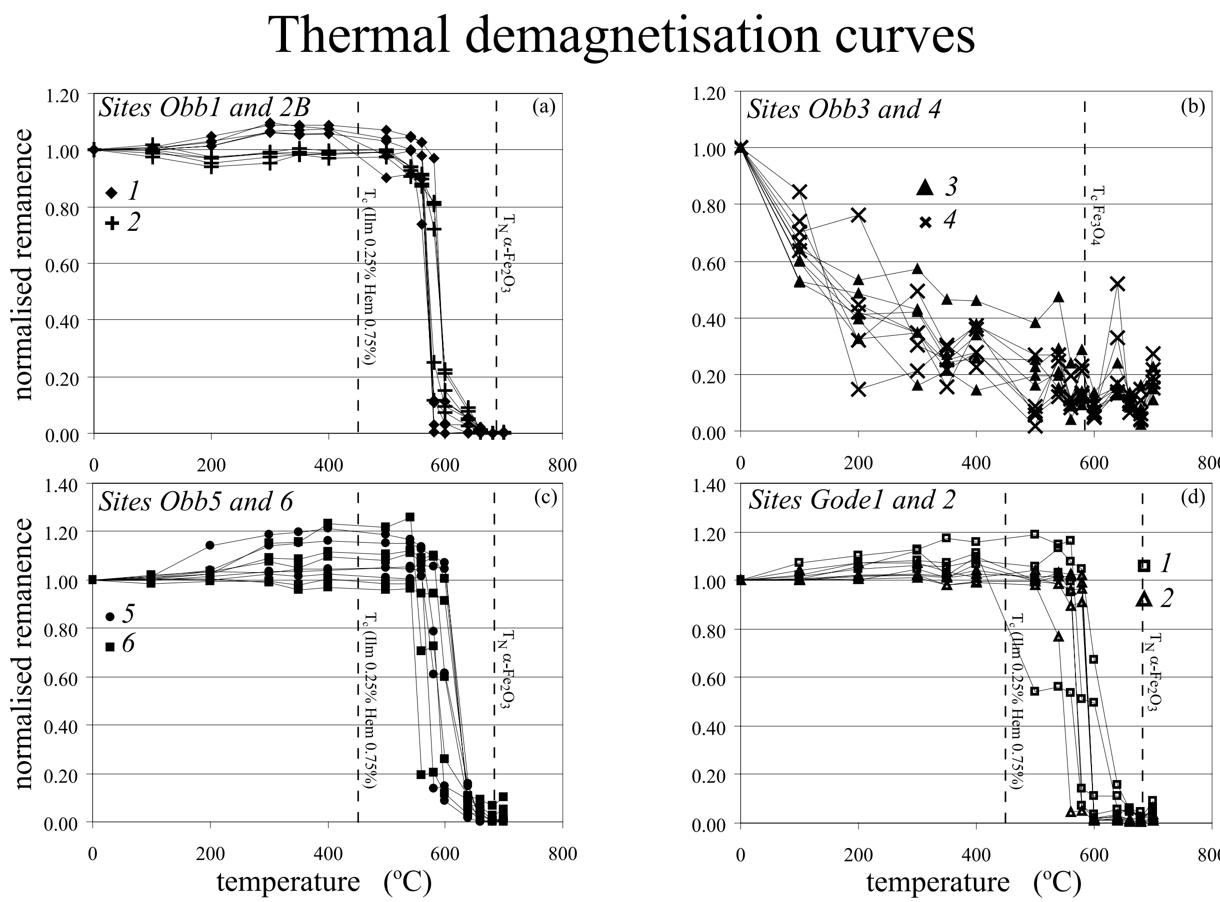

Figure 8. Remanent intensity as a function of temperature during demagnetization. The curves were normalized with the initial values before plotting. (a) Results from the sites OBB 1 and OBB 2. (b) Results from the sites OBB 3 and OBB 4. (c) Results from the sites OBB 5 and OBB 6. (d) Results from the sites GODE 1 and GODE 2.

[25] The samples from sites GODE 1 and GODE 2 behaved similarly to sites OBB 1, OBB 2B, OBB 5, and OBB 6. However, they did not contain a reversely directed low T_{ub} component the way OBB 5 and OBB 6 did. The NRM directions were somewhat shallower and more NW directed compared to the Obbhult sites (Table 3). For AF demagnetization we only calculated F_r values (not L, F_{ch} and H_c), which were 0.80 and 0.88 for GODE 1 and GODE 2, respectively. The L values from thermal demagnetization were somewhat lower compared to the Obbhult results, 0.51 for GODE 1 and 0.74 for GODE 2. These low values were associated with somewhat higher F_{chth} when compared to L, which in turn was caused by instabilities/minor components in the initial demagnetization steps up to 400°C, particularly in GODE 1 (see higher MAD compared to Obbhult). Samples from GODE 1 had distinctly lower T_{ub25} compared to all other sites, only 408°C. The low T_{ub} value was associated with the presence both of minor components with T_{ub} below the main T_{ub} interval, but also with a partial lowering of the main unblocking interval itself.

[26] We calculated two mean directions and two poles using the AF and thermal demagnetization data from Obbhult and Gödestad, respectively, and they are given in Table 3. Mean directions with $\alpha95$ confidence circles are shown in Figure 9. Component OBB HB was calculated with samples from sites OBB 1, OBB 2, OBB 2B, OBB 5, and OBB 6, whereas OBB MEAN was based on the corresponding sites. Component REV was calculated from the reverse directed low blocking components from sites OBB 5 and OBB 6. Component OBB LB was calculated with the data from sites OBB 3 and OBB 4, and component GODE HB was calculated with the data from GODE 1 and GODE 2. The OBB MEAN has plat/plong at 218°/−24.3° with a D_p/D_m of 9.4°/9.9°, and the VGP from Gödestad is situated at plat/plong 203°/−51° with a D_p/D_m of 4.4°/5.6°. These poles are shown in Figure 11.

6.2. NRM Intensity, Susceptibility, and Koenigsberger Ratio

[27] Values of χ are given in Table 4. Sites OBB 5 and particularly OBB 1 had the lowest χ ($\sim 1000 \times 10^{-6}$ SI). The samples from Gödestad had distinctly higher χ ($20{,}000 - 100{,}000 \times 10^{-6}$ SI), whereas extreme values were encountered in OBB 4 ($150{,}000 - 350{,}000 \times 10^{-6}$ SI). The parameter χ between 45,000 and 130,000 was found for OBB 3. Note that Figure 12 has a log-scale and that we also give the ranges of the values in Table 4. There was often a large spread of values within each site, and all samples had

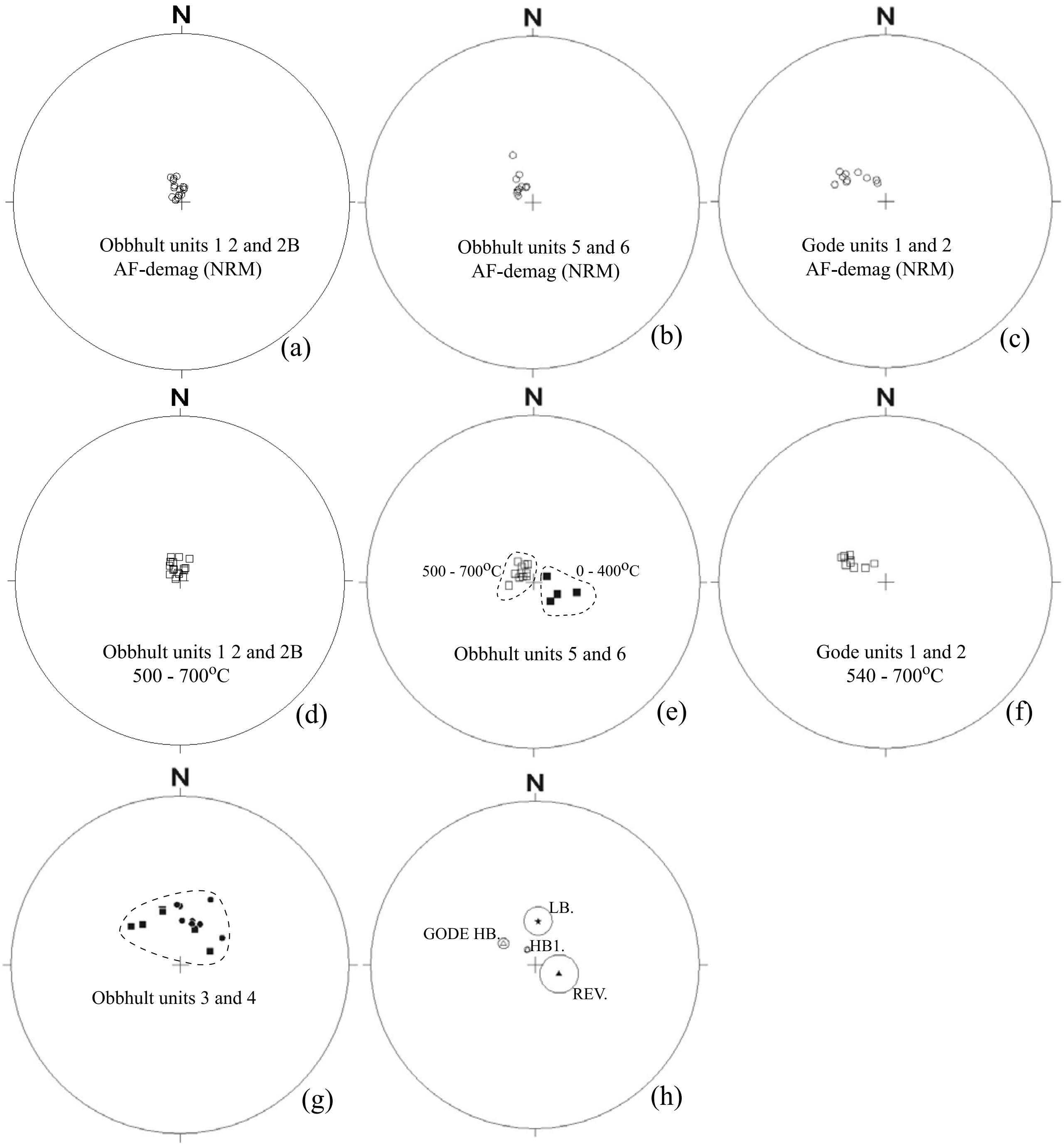

Figure 9. ChRM directions calculated with PCA and plotted in Wulff projections. The names of the sites are indicated in each stereoplot. Open symbols denote negative inclination and solid denote positive inclination. (a)–(c) AF results, (d)–(f) thermal results, (g) thermal and AF results from the sites OBB 3 and OBB 4, and (h) mean directions and 95% confidence circles (α95). See text for explanation of component names in Figure 9h (end of section 6.1).

NRM intensities in between ~0.3 and ~20 A/m, with distinct differences between the sites. Site OBB 2B had the highest NRM values, and the lowest were encountered in site OBB 3. To get an overview please see Table 4 or Figure 12. During measurement of samples from OBB L2, the 2G-SQUID gave to low and unreliable intensity data, whereas double checks of the directions with Molspin clearly indicated good directional stability. The OBB 2 intensity data must not be discussed, however, only OBB 2B.

[28] In Gödestad, the NRM intensity was approximately equal between GODE 1 and GODE 2 but the susceptibility was higher in GODE 1, and thus we also got lower Q values for GODE 1. Q for GODE 1 was 1.1 but for GODE 2 it was 7.2. Because χ varied much more than the NRM intensity, it

Table 2. Demagnetization Curve Parameters Calculated According to Section 5

Site	H_{c25}, mT	H_{c50}, mT	H_{c75}, mT	F_{chaf}[a]	F_{raf}[a]	L_{af}[a]	MAD_{af}[a]	T_{ub25}, °C	T_{ub50}, °C	T_{ub75}, °C	F_{chth}[a]	F_{rth}[a]	L_{th}[a]	MAD_{th}[a]
OBB 1					0.95			541	571	578	0.79	0.0024	0.77	0.90
OBB 2					0.94			573	591	603	0.72	0.0022	0.82	0.96
OBB 2B[d]					0.82			559	579	589	0.75	3.2×10^{-6}	0.83	1.6
OBB 3[b]	8.3	18	44	0.41	0.21	0.88	3.9	60	197	427		0.068	0.37	15
OBB 4[b]	6.3	13	27	0.66	0.030	0.89	3.2	76	214	434		0.058	0.24	7.0
OBB 5					0.918			565	591	610	0.75	0.0032	0.69	1.1
OBB 6					0.914			569	587	607	0.76	0.020	0.67	1.9
GODE 1					0.80			408	555	591	0.60	0.030	0.51	4.5
GODE 2					0.882			566	579	594	0.80	0.015	0.74	1.5

Site[c]	AF1, mT	AF2, mT	Stdav AF1	Stdav AF2	TH1, °C	TH2, °C	Stdav TH1	Stdav TH2
OBB 1					524	700	22	0
OBB 2					540	680	24	45
OBB 2B[d]								
OBB 3	13	90	11	43	0	572	0	18
OBB 4	8	113	5	75	0	300	0	0
OBB 5					568	680	18	45
OBB 6					556	700	36	0
GODE 1					548	660	18	55
GODE 2					552	700	11	0

[a]For each of the parameters the indexes were complemented with "af" or "th" to separate demagnetization techniques. Definitions were similar for each category, see section 5.
[b]All parameters in these column were calculated with the B method. The residual moment (**r**) was excluded during Hc calculations for these sites.
[c]The parameters in this heading refer to the site mean values of AF and thermal limits used during PCA, together with the standard deviations for these parameters.
[d]The site was measured with a Molspin magnetometer instead of a 2G-SQUID during demagnetization.

follows that the variation in Q was practically opposite to that of χ. Exceptional high Q values were found for the samples from OBB L1 and OBB L2 where we encountered 1500 and 1700 at a maximum, whereas OBB 4 had some exceptional low values, down to 0.065. The temperature dependencies of the susceptibility at low and high temperatures are shown in Figure 11, and there was a clear correlation between these results and the bulk susceptibilities. The four examples bulk values span over the whole susceptibility range encountered in all the sites, and therefore the data is representative of all cases. For the sample with the lowest susceptibility mostly paramagnetic behavior was encountered with a minor contribution of magnetite. Even though the bulk value for this sample was low, there was no considerable contribution from hematite, as seen from the absence of the Morin transition at ~260 K [*Morrish*, 1994]. The other samples had susceptibilities dominated by magnetite as evident from the large increases at the Verwey transition at ~120 K combined with Curie temperatures at ~585°C (Figure 11) [*Muxworthy and McClelland*, 2000; *Özdemir et al.*, 2002]. Some minor decreases at higher temperatures occur. These might represent small contributions from hematite, but they may also in deed be due to one of the two possible oxidation effects because of the heating (magnetite oxidizes to hematite and Fe silicates oxidizes to Fe oxides). The absence of the

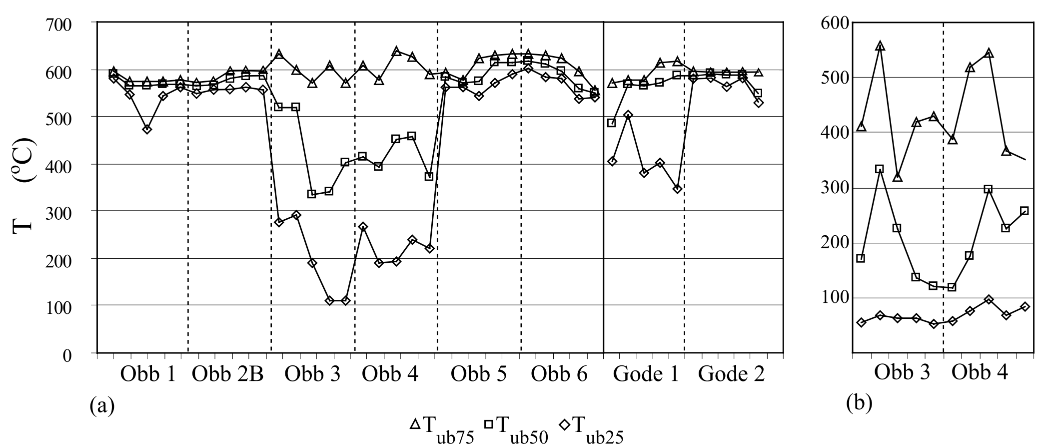

Figure 10. (a) Plot of the values T_{ub75}, T_{ub50}, and T_{ub25} for all samples. All the values were calculated with method A, and residual components were included in the denominator of equations (1)–(3). (b) Values from thermal demagnetization of sites OBB 3 and OBB 4, calculated with method B.

Table 3. Directions, Paleopoles, and Statistics for ChRM Components

Component	Dec/Inc[a]	N[b]	R[c]	k[d]	α95[e]	North Pole Latitude/Longitude[f]	South Pole[g]	D_p/D_m[h]
OBB LB NRM	7.2/68	19	17	11	10.7			
OBB LB	3.7/60.0	14	13	20	9.2	182/74 (VGP)	2/−74	11/14
OBB HB NRM	331/−78.7	50	50	105	2.0			
OBB 1	339/−75	10	10	513	2.1			
OBB 2	3.7/−80.4	11	11	283	2.7			
OBB 2B	323/−85.1	10	10	522	2.1			
OBB 5	311/−77.6	11	11	74	5.4			
OBB 6	324/−75.8	10	10	271	2.9			
OBB MEAN	332/−79.3	5	5	214	5.2	38.0/24.3 (paleopole)	218/−24.3	9.4/9.9
OBB HB	332/−79.3	52	52	118	1.8	38.0/24.3 (VGP)	218/−24.3	3.3/3.4
OBB REV	110.4/72.6	4	3.9	51	13	218/−51 (VGP)	38/51	21/23
GODE 1	301/−59.7	11	11	243	2.9			
GODE 2	311/−68.6	9	9	81	5.7			
GODE HB	304.5/−63.8	20	19.8	90	3.5	23/51 (VGP)	203/−51	4.4/5.6
GODE NRM	314.1/−62.6	20	20	64	4.1			

[a]Mean declination and inclination.
[b]Number of samples (for VGPs) or sites (for paleopoles).
[c]Precision parameter according to *Fisher* [1953].
[d]Precision parameter according to *Fisher* [1953].
[e]The 95% cone of confidence according to *Fisher* [1953].
[f]Paleopole position according to dipole model (for north pole).
[g]South pole choice for VGPs.
[h]Ovals of statistical confidence for VGPs.

Morin transition speaks against the possibility of initial hematite susceptibility contributions, however. The overall results, was thus that the susceptibilities in the samples were due to varying sample-specific contributions of multidomain (MD) magnetite with Fe silicate contributions occurring only in samples with low bulk values.

7. Discussion

7.1. Magnetic Phases and Their Properties

[29] A first step on the way to understand the causes for the anomaly could be to assess magnetic properties to different minerals and grain assemblages of varying sizes. A discussion of the magnetic mineral contents in the various rock formations must take into account both the demagnetization behavior, the directions, and the variations in intensive magnetic variables such as NRM intensity, χ, and Q values. An initial comparison of the demagnetization results from the rock formations indicated that the magnetic properties could be understood using few, (perhaps two or three) magnetic carriers of distinctly different character. The demagnetization curves for units OBB 1, OBB 2, OBB 2B, OBB 5, and OBB 6, together with GODE 1 and GODE 2 are rather similar with little loss of remanence during AF demagnetization, and discrete unblocking intervals in between 560 and 630°C during thermal demagnetization. OBB 3 and OBB 4 both had much lower coercivities and lower unblocking temperatures (Table 2 and Figure 10). The high coercivities seen during AF demagnetization in all sites (except OBB 3 and OBB 4), is an indication against magnetite as remanence carrier in these sites since magnetite usually has lower coercivity. Previous investigations at Gödestad, argued for nanometer-sized exsolved lamellae of intergrown hematite and ilmenite as magnetic carriers based on a magnetization measurement and TEM study [*McEnroe et al.*, 2001]. In our samples (OBB 1, OBB 2, OBB 2B, OBB 5, OBB 6, GODE 1, and GODE 2) we have both the same demagnetization behavior and the presence of similar hematite-ilmenite aggregates according to SEM. Thin lamellae occur as curved plates of an ilmenite rich phase inside the hematite rich lamellae (Figure 4). The widths of the thinnest lamellae were smaller than the best resolution of the SEM, and it is likely that the NRM of units OBB L1, OBB L2, OBB L5, and OBB L6 together with GODE 1 and GODE 2 is hosted in such oxide aggregates. The mechanism by which this type of NRM is maintained is debated [*Kletetschka et al.*, 2002; *McEnroe et al.*, 2004; *Burton et al.*, 2005]. Even though we cannot yet solve this question with our data and methods we now need to make a comment, because the unblocking temperatures were often confusingly close to the Curie temperature of magnetite.

[30] The remanence is likely associated with defects in the hematite. *McEnroe et al.* [2001] argued that the NRM is due to uncompensated spins at the interfaces between hematite and ilmenite and that these defect associated moments get important due to the high net surface areas of the lamellae intergrowths. An estimation of the typical number of μ_B per volume, as well as a magnetic measurement of the net magnetic moment of the material (as if no domain walls are present in those grains), remains to be done, however, making the interpretations controversial. The presence of a discrete unblocking temperature much lower than the Néel temperature of hematite (560–640°C compared to 680°C) was a characteristic feature in our samples. The main parts of the hematite grain lattices, must have lowered Néel temperature if some incorporation of titanium occurs, thereby lowering also the unblocking temperature for any defect related magnetic moments. An ideal and defect free hematite rich exsolved phase (titanohematite) is predicted to have low magnetic moment because it is an antiferromagnet, whereas the bulk of the ilmenite rich phase (hemo-ilmenite) is predicted to have

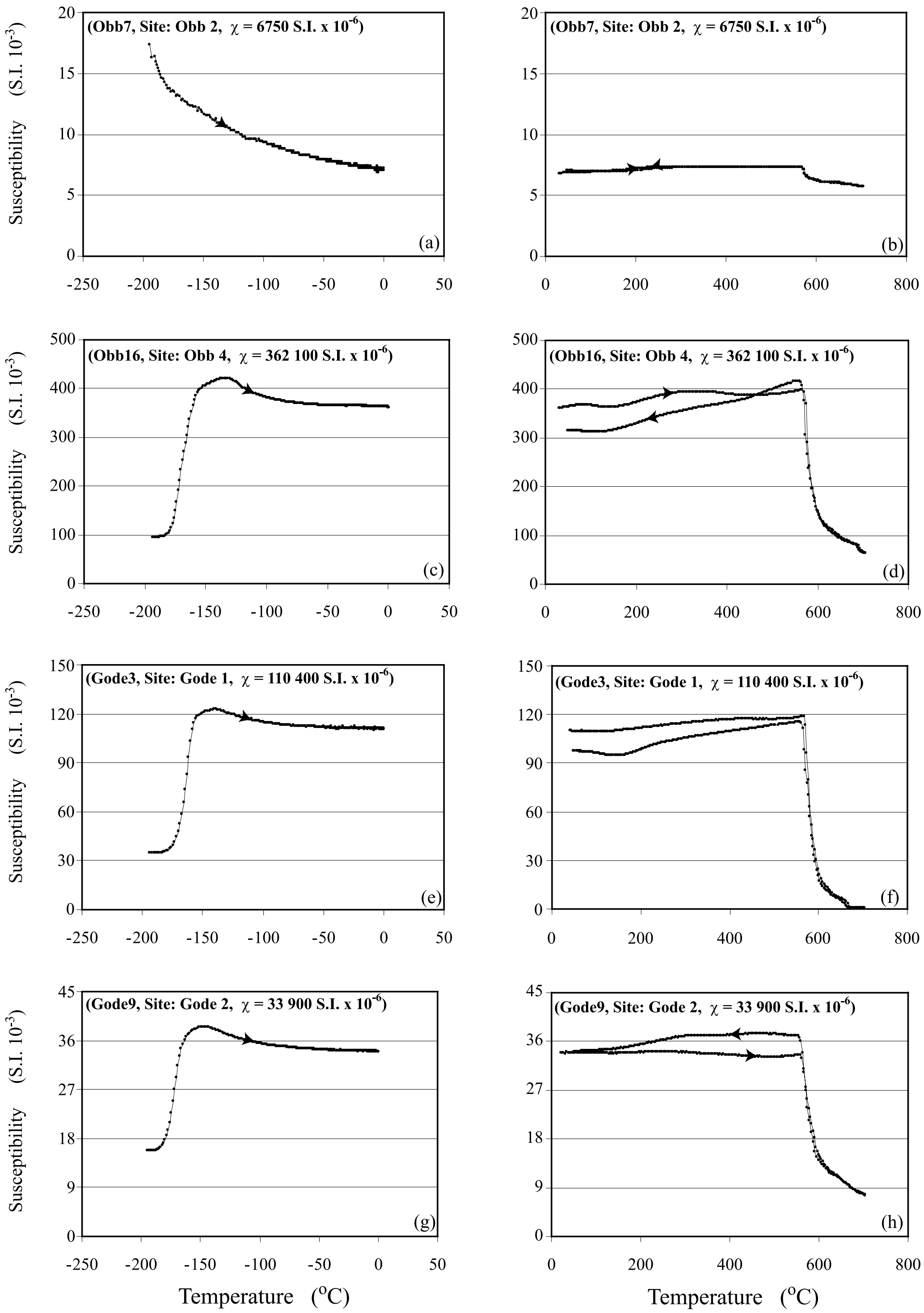

Figure 11. Weak field susceptibility as function of temperature during heating in air between −192 and 700°C. (a)–(b) Sample OBB 7 from unit OBB L2, (c)–(d) OBB 16 from unit OBB L2, (e)–(f) GODE 3 from unit GODE 1, and (g)–(h) sample GODE 9 from unit GODE 2.

zero remanence because of its cryogenic Curie temperature (below this temperature it is a ferrimagnet). If one does not accept defect related contributions to the magnetism, we would have to deal with either a phase of low net moment, or a phase with high net moment but with cryogenic Curie temperature [*Carmichael*, 1962; *Ishikawa*, 1962]. Our main conclusive point is thus only that magnetite is not needed to explain the unblocking temperatures. We will call this type of grains magnetic carriers of type 1.

[31] The units OBB 3 and OBB 4 were completely different with H_{c50} in between 10 and 20 mT, and T_{ub50} at ∼200°C (Figure 10 and Table 2). This strongly suggests multidomain (MD) magnetite as remanence carrier, because the interval 5–20 mT is lower than the assumed coercivity

Table 4. Bulk Rock Magnetic Parameters for the Obbhult and Gödestad Sites

Site	$\langle\chi\rangle$,[a] SI × 10^{-6}	Minimum χ[a]	Maximum χ[a]	$\langle$NRM$\rangle$,[b] mA/m	$\langle$NRM$\rangle$,[c] mA/m	Min. NRM[b]	Max. NRM[b]	$\langle$Q$\rangle$[d]	Minimum Q[d]	Maximum Q[d]
OBB 1	1,100	6.9	3,200	2,200	2,200	320	4,400	480	25	1500
OBB 2[g]	4,600	250	8,900	9,800	9,800	2,000	13,000	230	8.4	1300
OBB 2B[f]	2,900	290	8,700	16,000	16,000	12,000	20,000	480	42	1700
OBB 3	89,000	46,000	130,000	1,500	1,500	460	3,000	0.45	0.12	0.79
OBB 4	210,000	160,000	360,000	5,700	4,900	370	10,410	0.59	0.058	0.96
OBB 5	910	520	2,600	4,400	4,400	450	8,600	130	14	310
OBB 6	17,000	650	35,000	3,200	3,200	1,300	7,300	24	0.96	130
GODE 1	100,000	89,000	150,000	4,300	4,300	3,500	5,300	1.1	0.62	1.8
GODE 2	24,000	18,000	31,000	6,600	6,500	4,400	8,000	7.2	3.7	11
				Geometric Mean[e]						
OBB 1	240			1,700				180		
OBB 2[g]	3,000			8,500				71		
OBB 2B[f]	1,700			16,000				240		
OBB 3	85,000			1,300				0.38		
OBB 4	200,000			4,400				0.43		
OBB 5	870			3,500				88		
OBB 6	9,600			2,800				7.8		
GODE 1	100,000			4,300				1.1		
GODE 2	23,000			6,400				6.7		

[a]$\langle\chi\rangle$ denotes the mean value of volume susceptibility, and minimum χ and maximum χ are the range in χ.
[b]$\langle$NRM$\rangle$ is used for intensity mean values, and minimum NRM and maximum NRM are for ranges.
[c]Mean values of NRM according to equation (4).
[d]Q are mean values of Koenigsberger rations, and minimum Q and maximum Q are the ranges there of (geomagnetic field of 40.035 A/m assumed).
[e]Geometrical means are given instead of arithmetic.
[f]The site was demagnetized with a Molspin magnetometer due to high NRM values.
[g]Values of NRM and Q affected by high intensity NRM samples measured in 2G-SQUID.

due to magnetocrystalline anisotropy. The magnetocrystalline anisotropy puts a minimum value on the coercivity of single-domain (SD) grains (in practice, it would be higher due to shape anisotropy) [*Dunlop and Özdemir*, 1997], and thus it follows that demagnetization must have been due to domain wall translation during AF treatment. This is probably also reflected by low unblocking temperatures, that were ~350°C below the Curie temperature. Note that we rely on T_{ub} calculation with Method B for these sites. The reasons were instabilities in the demagnetization curves and

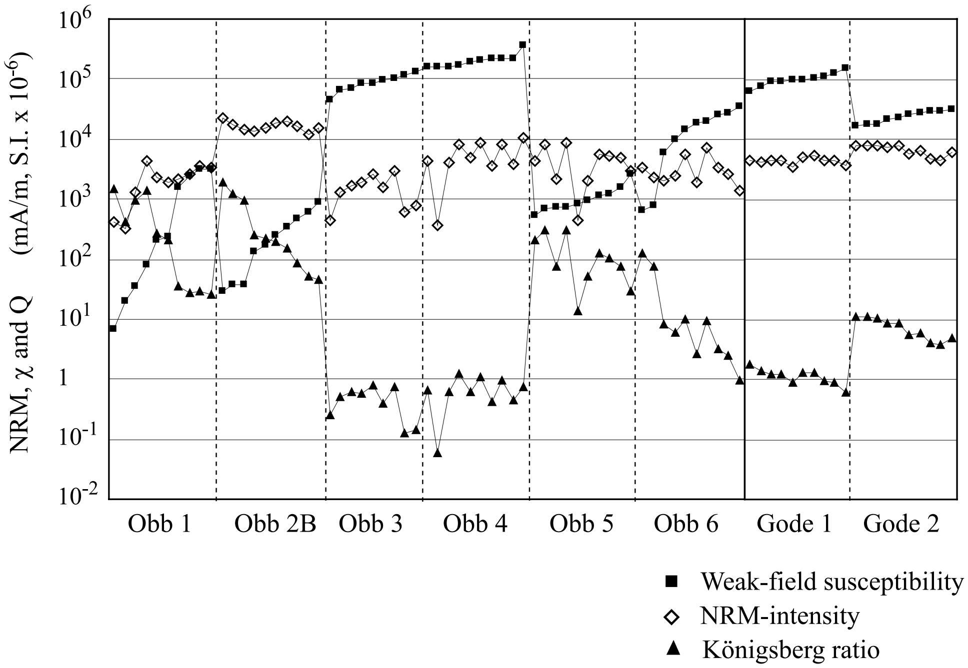

Figure 12. Weak field susceptibility, NRM intensity, and Koenigsberger ratio (Q) for all the samples. The scale to the left is common for all these parameters, but the unit for susceptibility is SI × 10^{-6}, and the unit for NRM is mA/m (Q is also read from the same scale, but it is dimensionless).

possible laboratory-induced components at high demagnetization temperatures. Pure magnetite grains of the approximate sizes 20–500 μm were also observed in the SEM, which supports our domain state interpretation together with the high-temperature susceptibility results. The grain sizes and the formation mechanisms of MD magnetite grains could be different in Gödestad and Obbhult, but because of their characteristic magnetic behavior we will now refer to them as type 2 carriers.

[32] Deviations from pure type 1 and type 2 behavior occur. In the site OBB 3, samples could have F_r components up to 20% (Figure 7b). These F_r components were fully isolated from the type 2 remanences following demagnetization at 40 mT, but they remained stable in direction and intensity up to 150 mT. Their endpoint directions were steep and directed toward north (we did not make statistics on these endpoint directions because they were to few). This is completely different when compared to the type 1 grains. In the SEM, we observed pure hematite with few or no ilmenite lamellae. These must be the carrier grains of the stable F_r components (the endpoints), and thus the OBB 3 samples represent an intermediate variety, seemingly with a physical mixture of type 1 and type 3 carriers. Type 3 magnetic grains do not dominate bulk magnetic properties in any of the samples.

[33] Another deviation from the pure type 1 or 2 behaviors occurs in the site GODE 1. During AF demagnetization there was demagnetization of a minor component with H_c at 10 mT, but after this there were no further changes of the remanence intensity or direction. A counterpart was seen in the intensity decreases at low temperatures during thermal demagnetization (Figure 8d). Again, a physical mixture is indicated but with type 1 (hematite-ilmenite) and 2 (MD magnetite) carriers, not type 3. We also see the presence of these components as small increases of the remanence in the AF results of Figure 7d (note that its scale is less expanded compared to Figures 7a and 7c). This increase is because of the large angle between the remanence directions associated with types 1 and 2 in site GODE 1. In Table 2 the phenomenon manifests as a lower L (0.51) and F_{ch} (0.60) during thermal demagnetization, when we compare to the sites with type 1 remanence only (remember it was the high-blocking type 1 remanence which was used as ChRM). The F_r values during AF demagnetization (0.80) were also the lowest found for all sites with type 1 remanence. In conclusion, we have seen rocks with type 1 magnetic carriers only (OBB 1, OBB 2, OBB 2B, OBB 5, OBB 6 and GODE 2). We have seen rocks with major type 1 and minor type 2 (GODE 1), rocks with minor type 3 and major type 2 (OBB 3), and last we have seen rocks with type 2 only (OBB 4).

[34] Now, we can compare the demagnetization results with values of NRM intensity χ and Q for the different sites. OBB 1, OBB 2B, OBB 5, and OBB 6 together with GODE 2 had the lowest susceptibilities and the highest Q values (Figure 12 and Table 4). None of these sites had any type 2 (MD) remanence during demagnetization (MD magnetite). GODE 1, which had 10–100 times higher χ also had some type 2 remanence but it was subordinate. OBB 3 had high susceptibility and ~20% type 3 (hematite) remanence at maximum, the rest was dominated by type 2 behavior. OBB 4, however, which had even 2 times higher χ than GODE 1 and OBB 3, only had remanence carriers of type 2. It is clear that the proportion of demagnetized type 2 remanence was correlated to the susceptibility. The susceptibility was due to MD magnetite, because there was no Hopkinson effect in the thermomagnetic curves. All this is consistent because the coercivity spectrum of the type 2 grains also indicated MD magnetite. The magnetite might not show up at all or just a little during demagnetization, even though it dominates the susceptibility completely. This is not only due to the proportions between the types 1 and 2 grains, but in deed also due to their respective relations between susceptibility and remanence properties (MD magnetite is an inefficient NRM carrier but has high susceptibility). For those sites, which only had type 2 magnetic grains according to demagnetization, we would expect a characteristic property also with respect to the NRM susceptibility or Q values. This also turned out to be the case. The mean Q values were closer to 0.5 for the sites OBB 3 and OBB 4, which is exactly the prediction for thermal remanent magnetization (TRM) in MD magnetite [*Stacey and Banerjee*, 1974] (Table 4). Furthermore, the much varying susceptibility was not correlated to as much varying NRM intensities. Therefore the main trends for Q were opposite to those for χ:

$$Q = \frac{|\mathbf{NRM}|}{\chi \cdot \mathbf{H}_{geo}} \tag{5}$$

In equation (5), H_{geo} represents the geomagnetic field. On the basis of our petrographic descriptions and the findings above, the susceptibilities must be due to combinations of the contributions from MD magnetite hematite-ilmenite and paramagnetic silicates, such as pyroxenes amphiboles and biotite. Assuming low amounts of noninteracting magnetite grains and no problematic correlations between grains sizes and magnetite amounts, one may propose the following equation for Q:

$$Q \propto \frac{|\mathrm{NRM_{Mt}} + \mathrm{NRM_{Hemilm}}|}{\left[x_{\mathrm{Mt}} \times \chi_{\mathrm{Mt}} + x_{\mathrm{Hemilm}} \times \chi_{\mathrm{Hemilm}} + x_{\mathrm{para}} \times \chi_{\mathrm{para}}\right] \mathrm{H_{geo}}} \tag{6}$$

In equation (6), x_{Mt}, x_{Hemilm} and x_{para} denote the volume concentrations of MD magnetite hematite-ilmenite and paramagnetic minerals, respectively. The indexed χ symbols denote the susceptibilities of these minerals (using some weighted average value for the paramagnetic phases). The sites OBB 5 and OBB 6 together with GODE 2, and particularly OBB 1 and OBB 2B have higher Q than the other sites due to low or zero x_{Mt} in equation (6), enabling the discussion of yet another interesting phenomenon, the internal Q variation in sites OBB 1 and OBB 2B. These contain extreme Q values, up to ~1700. They could be due to low values for the ratio x_{para}/x_{Hemilm}. The nominator is not affected by x_{para} for instance, because the NRM is only due to the hematite-ilmenite grains. The denominator on the contrary, could be affected by varying paramagnetic contents. If all the paramagnetic minerals were removed, the Q value in equation (6) would start to approach the Q value for a pure average hematite-ilmenite grain, which is an unknown high number. To see if this is the case, one must compare whole rock susceptibilities with the susceptibilities for bulk pyroxene. If the bulk rock values turn out to be much lower than that, then the variation in Q will be governed by the different depletion of paramagnetic contents in the samples [*Rochette*, 1987]. This is definitely consistent with the paramagnetic low-temperature susceptibility curves shown in Figure 11. The mean susceptibility of site OBB 1 was 1.1×10^{-3} SI or 0.24×10^{-3} SI (geometric mean), but the lowest value (corresponding to the 1500 Q sample of OBB 1) was 6.9×10^{-3} SI. That is only 4–6 per mil of the bulk susceptibility for orthopyroxene [*Hunt et al.*, 1995]. This is in agreement with our microscopy observation that dark rock forming silicates were rare in OBB L1 and partly also in OBB L2 (Figure 3). The NRM intensities themselves are indeed more geophysically important compared to these variations in Q, but the distinct behavior of the hematite-ilmenite grains, including their close to zero contribution to χ can be demonstrated this way with the site OBB 1. The conclusions merely demonstrate the complex rock magnetic properties of the granulites.

7.2. Origin of the Magnetic Phases

[35] The Fe-Ti oxide minerals in the Obbhult and Gödestad samples demonstrate different textural relationships, and there is also a marked variation in grain size from <30 μm to >3000 μm for single grains. Four textural types can be seen easily in thin sections. The most common one is more or less irregularly shaped hematite with ilmenite exsolution lamellae. The second is composite grains of magnetite and hematite. In layers OBB L4 and OBB L5 furthermore, the Fe-Ti oxides are to a large extent associated with corundum and sapphirine and they occur in elongated metamorphic reaction domains. The fourth textural type contains Fe-Ti oxides, occurring as crystallographically oriented inclusions mainly in orthopyroxene and sapphirine, and these may have formed due to exsolution processes or as epitactic grains. All rocks at Obbhult and Gödestad have been metamorphosed at high temperatures, and even though clear differences exist, it is less interesting to relate this to the magnetic results. A preliminary study based on just a few analyses indicated temperatures close to 800°C at pressures around 0.7 GPa (C. Möller, personal communication, 2002). The rocks are completely recrystallized and all silicate minerals, possibly with exception of the coarse-grained plagioclase in OBB L1, are of metamorphic origin. It is very difficult to know to what extent the Fe-Ti oxides are the result of the intense metamorphism or if any single oxide crystals physically "survived" the metamorphism and deformation. From a rock magnetic point of view it is clear that the thermal overprint during the high-temperature metamorphism must have erased any "memory" from premetamorphic stages.

7.3. Age of the ChRM Components

[36] In order to understand how the NRM was formed it is of interest to determine its age. The main purpose, however, was not to determine the APW path but to tie concepts related to regional geophysics and geology, to those magnetic properties that could be of interest for aeromagnetic anomalies. Therefore the discussion needs to be short and strict but still helpful for such specific purposes.

[37] The uplift which caused cooling through 500–350°C after the Sveconorwegian event occurred at 930 Ma, or possibly in the interval 930–900 Ma. This is the temperature interval of interest for paleomagnetism/rock magnetism, and we are primarily concerned with the acquisition of components OBB MEAN and GODE HB. There has been some uncertainty concerning the Sveconorwegian loop, which is seen as the approximate APW path outlined in Figure 13. *Walderhaug et al.* [1999] denied the existence of the loop due to the presence of a new pole from the Hunnedalen dikes at its southern apex (Figure 13 and Table 1). The Hunnedalen pole was assigned a relatively young age of 850 Ma, and thereby the northward continuation of the loop would be impossible. New Neoproterozoic data from the sedimentary Visingsö formation indicate, however, that the APW path still must approach the equator at some time after the Sveconorwegian orogeny [*Lewandowski et al.*, 2004]. *Pisarevsky and Bylund* [2006] furthermore, argued for a reestablishment of the loop. Our data do not exclude any of the existing interpretations. Regardless, there are several coeval poles that resemble our, so we argue that the ages of OBB MEAN and GODE HD is Sveconorwegian and that they are from the interval 900–950 Ma. Our poles, particularly the Gödestad pole are also correlated to the Egersund-Ogna anorthosite pole from southern Norway whose age was suggested to 950–900 Ma [*Brown and McEnroe*, 2004]. We remind that there could be some disturbance of the Obbhult pole due to late faulting (see geophysical background in section 2).

[38] *Walderhaug et al.* [2007] argue that Sveconorwegian granulites have high anisotropy, which has been indicated by AMS measurements, and that this could cause deflections of the NRM. However, such an argument is indirect because NRM and susceptibility are two different physical entities. Moreover, in Obbhult there are mixtures of MD magnetite and hematite-ilmenite of all proportions, but in neither case a sample has had its susceptibility dominated by hematite-ilmenite (which is the remanence carrier). Susceptibility has always been due to MD magnetite except where extreme Q values occurred. When this happened, the susceptibility seemed to be due to paramagnetic phases such as orthopyroxene. Therefore it seems that the AMS properties are uninteresting, at least in Obbhult and Gödestad.

[39] Generally, the investigation of rocks with regard to magnetization age benefits from a large geographical spread between sampled sites, but that is not the case with this study. Here we rather deal with rocks containing magnetic components of distinctively different blocking conditions and the relations between them could form an argument for their relative ages. These have become essential in the discussion and a larger geographic sampling area would therefore not be as helpful as in some other cases. Particularly, Ar-Ar ages show regional variation. Once one type of evidence is searched for other problems could appear, because geological events must not occur the same way in a larger area, and now, this leads over to a discussion of the OBB LB data.

[40] The component LB, which was found in sites OBB 3 and OBB 4 had the direction dec/inc 3.7°/60° and a paleopole at plat/plong −74°/2°, whereas *Bylund and Halvorsen* [1993] reported a Jurassic pole at plat./plong −69°/283°. That pole corresponds to an age of 180 Ma; however, the OBB LB pole is closer to the present magnetic South Pole, and therefore it must be younger than Jurassic. *Cederbom* [2002] discussed the possibility of a minor burial event

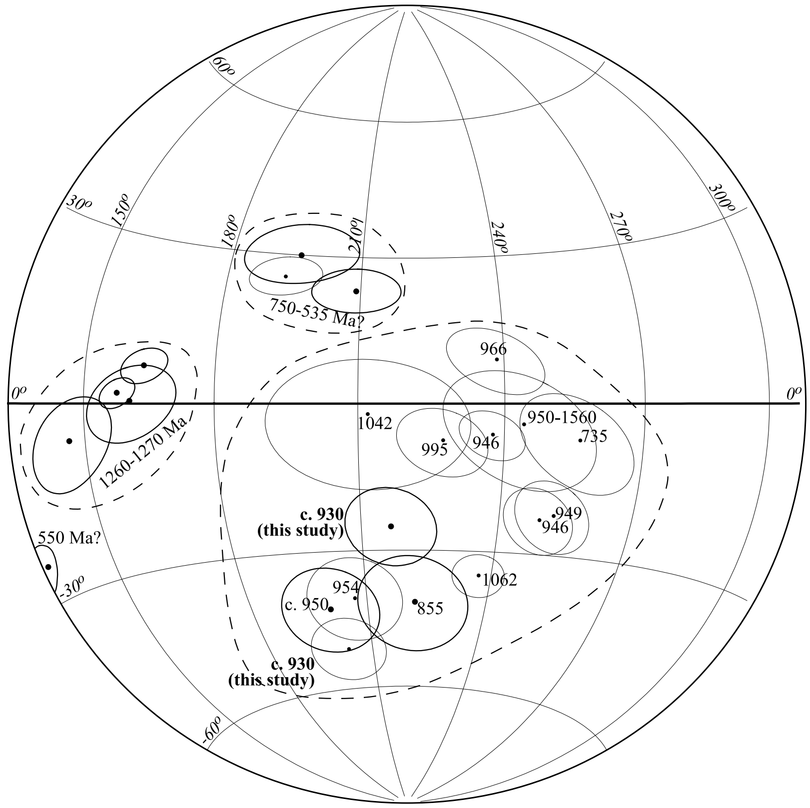

Figure 13. Paleopoles for the time interval shortly before, during, and shortly after the Sveconorwegian orogeny. The marked cluster at plat 0°, plong ~150° corresponds to the Saatakunta Igneous Complex in Finland and the Central Swedish Dolerite Group (CSDG). The marked cluster at plat ~30°, plong ~190° corresponds to Neoproterozoic poles from sedimentary rocks at the Varanger and Kola peninsulas. All the poles plotted here are also listed in Table 1.

during the Cretaceous-Paleogene in southern Sweden based on her fission track data. The LB pole is possibly related to this event. That is very much in agreement with the low T_{ub} values of the OBB LB component, which may suggest mild blocking conditions or unpinning of multidomains due to changed stress regimes. The declination of the OBB LB component is somewhat shallower than the present field at Obbhult and Gödestad (by ~10°) indicating that it is not entirely a viscous imprint of the present field.

7.4. Implications for the Origin of Local Anomalies

[41] Section 7.1 discussed different contents of magnetic phases and the different proportions with which they contribute to the remanence. The age of the high blocking component, which was carried by hematite-ilmenite was 900–950 Ma whereas the component in MD magnetite appeared to be Cretaceous. Since we know both the ages of the components, as well as their directions and now also due to our new classification method, their proportions in the samples, we will be able to support the discussion differently compared to previous studies. In a longer perspective such methods may answer critical questions about how magnetic anomalies arise (compare Figure 14).

[42] We shall now start our discussion of the OBB sites. One must bear in mind that the angle between the present field and the NRM components of sites OBB 3 and OBB 4 is small (~10°), whereas for all other sites it was 130–150°. The angles were estimated from the NRM directions in Table 3 and the value for the present inclination (~70°). The effects, which the varying magnetic properties could have on the anomaly, will depend both on these angles and the proportions of induced versus remanent magnetization. In Obbhult we got different results from granulites of different compositions. Five of the seven sites in Obbhult (OBB 1, OBB 2B, OBB 5, and OBB 6) gave completely remanence-dominated results with the high-angle 150° between the NRM and the present field, and this is combined with NRM

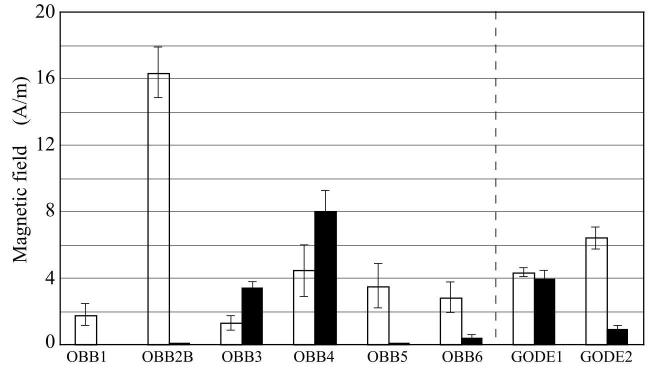

Figure 14. NRM intensity in (open bars), and induced magnetization (solid bars). The values are geometric mean values calculated from individual values for each sample within a site. The error bars show standard deviations.

intensities between 6 and 40% of the geomagnetic field. The magnetization from these rock units must contribute to the attenuation of the geomagnetic field at least for the OBB sites that are located in the middle of the GOA.

[43] With our new method for determination of F_{ch} we have proven that the magnetization, which was used to calculate the paleopole in Figure 13, constitutes 70–80% of the total remanence (Table 2). So, it is evident that 70–80% of the NRM in Figure 14 is Sveconorwegian, and the geophysical property, which could contribute to the GOA is hence also Sveconorwegian. However, both OBB 3 and OBB 4 have induced fields parallel to the geomagnetic field comparable in magnitude to the NRM components in some of the HB dominated sites. OBB 4 had a total magnetization corresponding to ~15% of the geomagnetic field (induced plus remanent). This magnetic contribution is nearly parallel to the geomagnetic field. It seems that the granulites from the GOA represent extreme opposites with respect to geophysical behavior. The presence of such rocks might explain the sharp peaks of small positive anomalies (positive relative to the GOA itself but not relative to the regional field) (Figures 2c–2e). The total volume of these rocks in Obbhult, however, was smaller compared to the rocks with strong Sveconorwegian remanence and negative inclinations. In Table 4, we gave not only conventional mean NRM intensities but also, intensity values calculated by vector addition. Analogously with this it is possible to calculate a vector based mean intensity and direction for the OBB sites including both MD magnetite and hematite-ilmenite dominated rocks (equation (4)). Doing so, we arrived at a mean magnetization of 3.5 A/m in the direction 336/−74. Adding also vector mean induced components the result will be 1.65 A/m but the direction changes with less than 1°.

[44] A different pattern was seen in Gödestad due to the metamorphic retrogression, which has led to a much more amphibole rich and garnet depleted rock locally (GODE 1). Gödestad is situated outside the GOA, which might have been missed in previous publications [*McEnroe et al.*, 2001]. It is not possible to use the data presented here to make models of the geomagnetic variations, but nevertheless it is essential to make a first attempt to characterize the surroundings of the GOA in terms of rock magnetic properties in order to indicate why the whole anomaly occurs.

[45] In Gödestad, we obtained Sveconorwegian ChRM with F_{ch} ratios of 60 and 80% for GODE 1 and GODE 2, respectively. When it comes to GODE 2 the picture is simply the same as for OBB 1, OBB 2B, OBB 5, and OBB 6. GODE 2 type granulites could only have a canceling effect on the geomagnetic field, whereas the retrogressed GODE 1 must be nearly indifferent in this respect (Figure 14). The induced magnetization is of the same magnitude as the NRM, but their directions are almost opposite (130°). Thus it seems that the retrogressive metamorphism has altered the oxide mineral compositions to give a rock, which contributes much less or nothing to the GOA anomaly. However, this is also dependent on the today's situation with Sveconorwegian ChRM directions combined with the induced field directions. That is consistent with the lower F_{ch} value for the Sveconorwegian ChRM (60% compared to 80% for GODE 2). We identified the breakdown of garnet with subsequent formation of magnetite during the metamorphic retrogression in GODE 1 (section 4). That is probably one part of the explanation. However, the amount relations between magnetite and hematite-ilmenite were likely also affected by crystallization of amphibole, which can contain more titanium compared to orthopyroxene and clinopyroxene. This reaction has likely favored magnetite on the expense of hematite-ilmenite.

[46] Eventually, two factors/processes have been identified, that diminish the effect of the strong and stable Sveconorwegian remanence in the area. The first is the presence of minor units of differing bulk composition with high amounts of MD magnetite (OBB 4 which is an Al-enriched variety and OBB 3). The second factor is retrogression of granulite to amphibolite (GODE 2 becomes GODE 1 type). We still argue that the GOA is due to the strong Sveconorwegian ChRM, but the total picture and internal variations were more complex than previously believed. Last we point out that the GOA anomaly is ~5 km wide and 20 km long. The width 5 km is quite small compared to what would be expected if it originated at lower or mid levels in the crust. Therefore this particular anomaly cannot provide evidence of deep-seated anomalies, for instance, on Mars [cf. *Robinson et al.*, 2002].

8. Conclusions

[47] 1. Two new methods were defined to calculate paleomagnetic unblocking data. The A method is based on subdivision of the vector difference sum in 25, 50, and 75% quartiles. The B method consists of the calculation of median destructive fields (MDF), but not only 50% were calculated, also 25 and 75% values.

[48] 2. The A and B methods were successfully applied to characterize rock magnetic properties of granulites. The A method was successfully applied to components associated with exsolved hematite-ilmenite, but the B method was needed for components associated with MD magnetite because of unstable behavior.

[49] 3. Magnetic properties of rocks in and around the GOA are due to different proportions of exsolved hematite-ilmenite combined with MD magnetite, but the exsolved hematite-ilmenite causes the negative aeromagnetic anomaly.

[50] 4. In Gödestad, there were NRMs with 60–80% hematite-ilmenite contributions, and in Obbhult, there were NRMs 0–80% hematite-ilmenite contributions. The paleopoles mentioned under 6.) (below) were calculated from sites all having 60% or more hematite-ilmenite components. This gives quantitative assignment of ages to partial components.

[51] 5. Unblocking characteristics were as follows: Exsolved hematite-ilmenite dominated samples had all T_{ub} quartiles (T_{ub25}–T_{ub75}) between 540 and 595°C, and H_{c25}-H_{c75} values much in excess of 150 mT. MD magnetite had T_{ub} values between 60 and 430°C and H_c values between 6 and 45 mT. The results thus represent a situation of no overlap between partial components.

[52] 6. Comparison between demagnetized MD magnetite content and bulk susceptibility could be made. About 40% MD magnetite corresponded to susceptibilities high enough to make the induced magnetization comparable in magnitude to the NRM (they were due to MD magnetite in almost all samples). The directions of the induced and remanent magnetizations were almost opposite (separated by 130–150°).

[53] 7. In Gödestad the proportion of MD magnetite increases with increased retrograde metamorphism. In Obbhult, there were more varying proportions but due to different bulk compositions instead. Altogether, this implies a more complex/varied origin for the GOA compared to previous models.

[54] 8. Three poles were reported: (1) plat/plong (218°/−24.3°) with D_p/D_m equal to (9.4°/9.9°) based on four sites in Obbhult (paleopole), (2) plat/plong (203°/−51°) with D_p/D_m equal to (4.4°/5.6°) based on two sites in Gödestad (VGP) (both of these are uplift poles associated with hematite-ilmenite, and their approximate age is 930 Ma), and (3) plat/plong 2°/−74° with D_p/D_m equal to 11°/14°. This pole was based on sites from Obbhult with abundant MD magnetite. Its age is less certain, possibly regarded as a maximum age, but it is most likely Cretaceous-Paleogene.

[55] **Acknowledgments.** Ildiko Antal-Lundin at the geological survey of Sweden helped us with the aeromagnetic data. Ann-Sofie Sidgren and Lina Åberg, Lund University, demagnetized the samples. This research is financed by the Geological Survey of Sweden (SGU). Charlotte Möller at SGU provided necessary unpublished data (datings, preinvestigations in Obbhult, etc.). Randolph Enkin provided valuable help as a reviewer, but the anonymous reviewers are also thanked.

References

Ade-Hall, J. M. (1969), Opaque petrology and the stability of natural remanent magnetism in basaltic rocks, *Geophys. J. R. Astron. Soc.*, *18*, 93–107.

Andersen, T. (2005), Terrane analysis, regional nomenclature and crustal evolution in the southwest Scandinavian Domain of the Fennoscandian Shield, *Geol. Foeren. Stockholm Foerh.*, *127*, 159–168.

Brown, L. L., and S. A. McEnroe (2004), Palaeomagnetism of the Egersund-Ogna anorthosite, Rogaland, Norway, and the position of Fennocandia in the Late Proterozoic, *Geophys. J. Int.*, *158*, 488–497.

Buchan, K. L., S. Mertanen, R. G. Park, L. J. Pesonen, S.-Å. Elming, N. Abrahamsen, and G. Bylund (2000), Comparing the drift of Laurentia and Baltica in the Proterozoic: The importance of key palaeomagnetic poles, *Tectonophysics*, *319*, 167–198.

Burton, B. P., A. Chaka, and D. J. Singh (2005), Chemical, magnetic and charge ordering in the system hematite-ilmenite, Fe_2O_3–$FeTiO_3$, *Phase Transitions*, *78*(1–3), 239–249.

Bylund, G. (1992), Palaeomagnetism, mafic dykes and the Protogine Zone, southern Sweden, *Tectonophysics*, *201*, 49–63.

Bylund, G. (1994), Palaeomagnetism of the Late Precambrian Vadsø and Barents Sea groups, Varanger Peninsula, Norway, *Precambrian Res.*, *69*, 81–93.

Bylund, G., and E. Halvorsen (1993), Palaeomagnetic study of Mesozoic basalts from Scania, southernmost Sweden, *Geophys. J. Int.*, *114*, 138–144.

Caratori Tontini, F. (2005), Stable inverse deconvolution of magnetic data, *Geophys. J. Int.*, *162*, 725–735.

Carmichael, C. M. (1962), The magnetization of solid solutions of ilmenite in hematite, *J. Phys. Soc. Jpn., Suppl.*, 711–713.

Cederbom, C. (2002), The thermotectonic development of southern Sweden during Mesozoic and Cenozoic time, in *Exhumation of the North Atlantic Margin: Timing, Mechanisms and Implications for Petroleum Exploration*, edited by A. G. Doré et al., *Geol. Soc. Spec. Publ.*, *196*, 169–182.

Dunlop, D. J., and Ö. Özdemir (1997), *Rock magnetism - fundamentals and frontiers*, 1st ed., 573 pp., Cambridge Univ. Press, Cambridge, U.K.

Elming, S. Å., and H. Mattsson (2001), Post Jotnian basic intrusions in the Fennoscandian Shield, and the break up of Baltica from Laurentia: A palaeomagnetic and AMS study, *Precambrian Res.*, *108*, 215–236.

Fisher, R. (1953), Dispersion on a sphere, *Proc. R. Soc. London, Ser. A*, *217*, 295–305.

Harrison, R. J., H. J. Stone, and S. A. T. Redfern (2006), Pressure dependence of Fe-Ti order in the ilmenite-hematite solid solution: Implications for the origin of lower crustal magnetization, *Phys. Earth Planet. Inter.*, *154*, 266–275.

Hunt, C. P., B. M. Moskowitz, and S. K. Banerjee (1995), Magnetic properties of rocks and minerals, in *Rock Physics and Phase Relations: A Handbook of Physical Constants*, *Ref. Shelf*, vol. 3, edited by T. J. Arhens, pp. 189–204, AGU, Washington, D. C.

Ishikawa, Y. (1962), Magnetic properties of hematite-ilmenite system at low temperature, *J. Phys. Soc. Jpn.*, *17*(B-I), 239–243.

Johansson, L., C. Möller, and U. Söderlund (2001), Geochronology of eclogite facies metamorphism in the Sveconorwegian Province of SW Sweden, *Precambrian Res.*, *106*, 261–275.

Kasama, T., S. A. McEnroe, N. Ozaki, T. Kogure, and A. Putnis (2004), Effects of nanoscale exsolution in hematite-ilmenite on the acquisition of stable natural remanent magnetisation, *Earth Planet. Sci. Lett.*, *224*, 461–475.

Kletetschka, G., P. J. Wasilewski, and P. J. Taylor (2002), The role of hematite-ilmenite solid solution in the production of magnetic anomalies in ground-and satellite-based data, *Tectonophysics*, *347*, 167–177.

Kretz, R. (1983), Symbols for rock-forming minerals, *Am. Mineral.*, *68*, 277–279.

Lewandowski, M., K. Malkowski, M. Moczydlowska-Vidal, M. Sidorczuk, and N. Abrahamsen (2004), Neoproterozoic paleogeography and environment of the Visingsö basin (southern Sweden) Evidence from palaeomagnetism and stable isotopes, paper presented at the 5th Nordic Palaeomagnetic Workshop, Geol. Surv. of Fin., Espoo, 25–29 Sept.

McDougall, I., and T. M. Harrison (Eds.) (1988), *Geochronology and Thermochronology by the $^{40}Ar/^{39}Ar$ Method*, 1st ed., 207 pp., Oxford Univ. Press, New York.

McEnroe, S. A., R. J. Harrison, P. Robinson, U. Golla, and M. J. Jercinovic (2001), Effect of fine scale microstructures in titanohematite on the acquisition and stability of natural remanent magnetization in granulite facies metamorphic rocks, southwest Sweden: Implications for crustal magnetism, *J. Geophys. Res.*, *106*(B12), 30,523–30,546.

McEnroe, S. A., F. Langenhorst, P. Robinson, G. D. Bromiley, and C. S. J. Shaw (2004), What is magnetic in the lower crust?, *Earth Planet. Sci. Lett.*, *226*, 175–192.

Merrill, R. T. (1968), A possible source for the coercivity of ilmenite-hematite minerals, *J. Geomagn. Geoelectr.*, *20*(3), 181–185.

Mertanen, S., L. J. Pesonen, and H. Huhma (1996), Palaeomagnetism and Sm-Nd ages of the Neoproterozoic diabse dykes in Laanila and Kautokeino, northern Fennoscandia, in *Precambrian Crustal Evolution in the North Atlantic Region*, edited by T. S. Brewer, *Geol. Soc. Spec. Publ.*, *112*, 331–358.

Möller, C. (1998), Decompressed eclogites in the Sveconorwegian (-Grenvillian) orogen of SW Sweden: Petrology and tectonic implications, *J. Metamorph. Geol.*, *16*, 641–656.

Möller, C., J. Andersson, U. Söderlund, and L. Johansson (1997), A Sveconorwegian deformation zone (system?) within the eastern segment, Sveconorwegian orogen of SW Sweden—A first report, *Geol. Foeren. Stockholm Foerh.*, *119*, 1–12.

Morrish, A. H. (1994), *Canted Antiferromagnetism: Hematite*, 192 pp., World Sci., Singapore.

Muxworthy, A. R., and E. McClelland (2000), Review of the low-temperature magnetic properties of magnetite from a rock magnetic perspective, *Geophys. J. Int.*, *140*, 101–114.

Neuvonen, K. J. (1966), Palaeomagnetism of the dike systems in Finland, II, Remanent magnetization of dolerites in the Vaasa archipelago, *C. R. Soc. Geol. Fin.*, *38*, 275–281.

Neuvonen, K. J., and L. Grundström (1969), Palaeomagnetism of the dike systems in Finland, IV, Remanent magnetization of the dolerite and related dikes in the Åland archipelago, *Bull. Geol. Soc. Fin.*, *41*, 57–63.

Özdemir, Ö., D. J. Dunlop, and B. M. Moskowitz (2002), Changes in remanence, coercivity and domain state at low temperature in magnetite, *Earth Planet. Sci. Lett.*, *194*, 343–358.

Page, L. M., C. Möller, and L. Johansson (1996), ^{40}Ar-^{39}Ar geochronology across the mylonite zone and the southwestern Granulite Province in the Sveconorwegian Orogen of SW Sweden, *Precambrian Res.*, *79*, 239–259.

Patchett, P. J., and G. Bylund (1977), Age of Grenville Belt magnetisation: Rp-Sr and Palaeomagnetic evidence from Swedish dolerites, *Earth Planet. Sci. Lett.*, *35*, 92–104.

Pedersen, L. (1985), The gravity and magnetic field for ellipsoidal bodies in the wavenumber domain, *Geophys. Prospect.*, *33*, 263–281.

Petrova, G. N. (1961), Various laboratory methods of determining the geomagnetic stability of rocks, *Bull. Acad. Sci. USSR, Geophys. Ser.*, 703–709.

Piper, J. D. A. (1980), A palaeomagnetic study of Svecofennian basic rocks: Middle Proterozoic configuration of the Fennoscandian, Laurentian and Siberian shields, *Phys. Earth Planet. Inter.*, *23*, 165–187.

Pisarevsky, S. A., and G. Bylund (2006), Paleomagnetism of 935 Ma mafic dykes in southern Sweden and implications for the Sveconorwegian Loop, *Geophys. J. Int.*, *166*, 1095–1104.

Popov, V., A. Iosifidi, A. Khramov, J. Tait, and V. Bachtadse (2002), Paleomagnetism of Upper Vendian sediments from the Winter Coast, White Sea region, Russia: Implications for the paleogeography of Baltica

during Neoproterozoic times, *J. Geophys. Res.*, *107*(B11), 2315, doi:10.1029/2001JB001607.
Robinson, P., R. J. Harrison, S. A. McEnroe, and R. A. Hargraves (2002), Lamellar magnetism in the haematite-ilmenite series as an explanation for strong remanent magnetization, *Nature*, *418*, 517–520.
Rochette, P. (1987), Magnetic susceptibility of the rock matrix related to magnetic fabric studies, *J. Struct. Geol.*, *9*(8), 1015–1020.
Shipunov, S. V., and N. M. Chumakov (1991), Palaeomagnetism of Upper Proterozoic deposits of the Kola Peninsula, *Geotectonics*, *25*(5), 401–410.
Stacey, F. D., and S. K. Banerjee (1974), *The Physical Principles of Rock Magnetism*, 195 pp., Elsevier, Amsterdam, Netherlands.
Söderlund, U., C. E. Isachsen, G. Bylund, L. M. Heaman, P. J. Patchett, J. D. Vervoort, and U. Andersson (2005), U-Pb baddelyite ages and Hf, Nd isotope chemistry constraining repeated mafic magmatism in the Fennoscandian Shield from 1.6 to 0.9 Ga, *Contrib. Mineral. Petrol.*, *150*(2), 174–194.
Tauxe, L. (1998), *Palaeomagnetic Principles and Practice*, *Mod. Approaches Geophys.*, vol. 17, 300 pp., Kluwer Acad., Dordrecht, Netherlands.
Torsvik, T. H., D. Roberts, and A. Siedlecka (1995), Palaeomagnetic data from sedimentary rocks and dolerite dykes, Kildin Island, Rybachi, Sredni and Varanger peninsulas, NW Russia and NE Norway: A review, in *Geology of the Eastern Finnmark: Western Kola Peninsula Region*, edited by D. Roberts and Ø. Nordgulen, *Norg. Geol. Unders. Spec. Publ.*, *7*, 315–326.
Walderhaug, H. J., T. H. Torsvik, E. A. Eide, B. Sundvoll, and B. Bingen (1999), Geochronology and palaeomagnetism of the Hunnedalen dykes, SW Norway: Implications for the Sveconorwegian apparent polar wander loop, *Earth Planet. Sci. Lett.*, *169*, 71–83.
Walderhaug, H. J., T. H. Torsvik, and E. Halvorsen (2007), The Egersund dykes (SW Norway): A robust early Ediacaran (Vendian) palaeomagnetic pole from Baltica, *Geophys. J. Int.*, *168*, 935–948.
Wang, X. D., U. Söderlund, A. Lindh, and L. Johansson (1998), U-Pb and Sm-Nd dating of high-pressure granulite- and upper amphibolite facies rocks from SW Sweden, *Precambrian Res.*, *92*, 319–339.

E. Eneroth and L. Johansson, GeoBiosphere Science Centre, Department of Geology, Lund University, Sölvegatan 12, SE-223 62 Lund, Sweden. (erik.eneroth@geol.lu.se)